135-m Meteorological Masts at the National Wind Technology Center

– Instrumentation, Data Acquisition and Processing –

Andrew Clifton

DRAFT, July 2014

Executive Summary

Two, 135 m-tall masts were erected at the National Renewable Energy Laboratory (NREL) National Wind Technology Center (NWTC) near Boulder, Colorado in 2010 and commissioned in a process that started early 2011. The masts were installed to support instrumentation to measure the inflow wind into two utility scale turbines at the NWTC. The construction, operation, and maintenance of the masts are supported through the Department of Energy's Office of Energy Efficiency and Renewable Energy, Wind and Water Power Program.

This document describes the status of the inflow monitoring masts on June 1, 2013. The document covers:

- An introduction to the winds at the NWTC
- The physical characteristics of the masts
- The instrumentation that has been installed
- Data processing methods
- Validation results

Figure 1. Wind turbines and meteorological masts at the National Wind Technology Center. One of the new 135-m masts is shown on the left of the photo, upwind of a wind turbine. Photo by Dennis Schroeder, NREL/PIX 19015.

Contents

List of Figures

List of Tables

1 About this document

This document has the following purposes:

1. Document the meteorological masts in their commissioned state in mid 2013.
2. Provide a reference detailing calculation methods
3. Provide a reference to other relevant documents

The reader is reminded that the mast instrumentation and the associated data processing software will be updated or changed periodically. The reader is therefore recommended to check that they are reading the most recent version of this document by comparing it to the NREL publications database at `http:www.nrel.gov`. Also, because data products may change, the reader is also suggested to check that the data they are using are up-to-date by comparing them with the data available online.

2 Project Objectives and Requirements

The objectives of the 135-m meteorological mast installation project include:

1. Measure the inflow to utility scale turbines with high spatial and temporal resolution.
2. Record data that can be used to quantify 3-dimensional turbulence and atmospheric stability across the atmospheric boundary layer and turbine rotor.
3. Provide high-quality data to researchers within and outside NREL and the wind energy community.

The above project objectives give rise to requirements for the masts. These requirements include:

1. Develop a set of instruments that quantify inflow winds and the atmosphere with high fidelity and resolution:
    A. Quantify inflow from the ground to the blade tip of a utility-scale wind turbine, at approximately 135 m above ground.
    B. Acquire and store multi-channel meteorological data at a sustained 20 Hz sampling rate
    C. Timestamp data with a GPS-derived time to allow comparison to other systems at the NWTC
2. Monitor the status of the data acquisition hardware and software in close-to-realtime:
    A. Include data from instrumentation such as power supply state, error codes and proper function.
    B. Create rules-based software to check and quantify the quality of measurements coming from the mast.
    C. Create software to ingest and display data from the measurements from each mast, including complex atmospheric data such as stability measures that may require data from multiple instruments.

3 Tower locations

3.1 The National Wind Technology Center

The inflow towers have been installed at the National Renewable Energy Laboratory's National Wind Technology Center (NWTC). The NWTC is approximately 8 km (5 miles) south of Boulder, Colorado, 36 km (20 miles) north west of Denver. It is situated about 5 km to the east of the Colorado Front Range at an elevation of approximately 1850 m (6,000 feet) above sea level.

3.2 Mast sites

The M4 and M5 towers are located on the eastern side of the NWTC grounds. The towers are positioned to the west of the utility-scale turbine test pads (Figure 2). In these locations they are approximately 2 rotor-diameters away from the utility-scale turbines, and are upwind in the prevailing wind direction (Figure 3).

3.3 The local wind climate

A long-term wind time series is available from the M2 mast at the west end of the NWTC (Figure 2). That time series extends from 1996 to the present day and can be found online at `http://www.nrel.gov/midc/nwtc_m2/`. Analysis of the long-term record shows that winds at the NWTC are dominated by west-north-westerly (WNW) flows. These WNW flows come from Eldorado Canyon, a prominent canyon approximately 5 km upwind (Figure 3).The WNW winds are frequent during the winter and early evenings; weaker winds may be katabatic winds or drainage flows (Banta et al., 1993), while stronger winds are associated with winter storms, and the Chinook. Winds from the north and south are also seen on site during summer time, and those winds may be driven by local thermally-driven circulation.

A data-mining technique called '*k*-means clustering' was used to analyse the winds at the NWTC by Clifton and Lundquist (2012). This analysis found that winds at the NWTC could be grouped into 4 clusters of representative wind speeds and directions. These clusters were southerly winds, northerly winds, weak westerly winds, and strong westerly winds. Similar clusters were found at all levels on the M2 mast. The wind speed and frequency of the clusters that were found at 80 m above ground are shown in Figure 4. The NWTC's winter 'wind season', when stronger winds are seen from the west, is clearly visible in the monthly data for November through April.

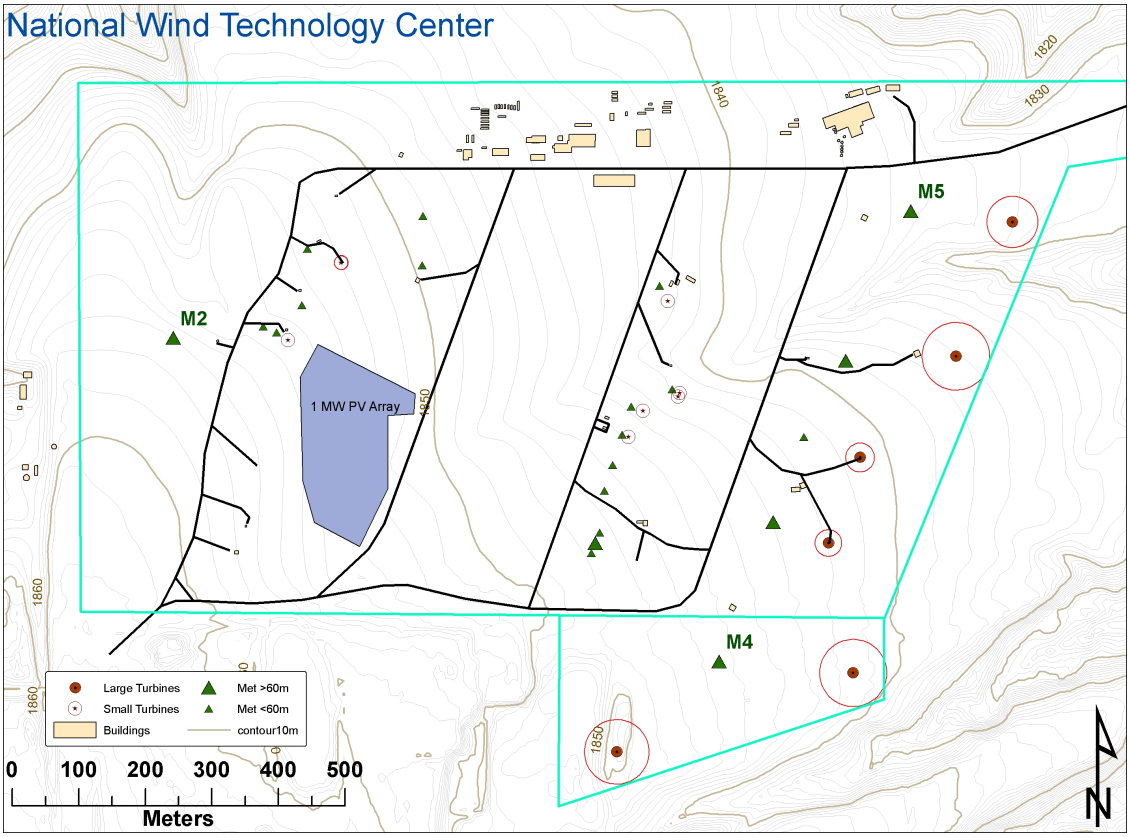

Figure 2. Location of wind turbines and meteorological monitoring towers at the NWTC. Figure courtesy Joe Smith, NREL.

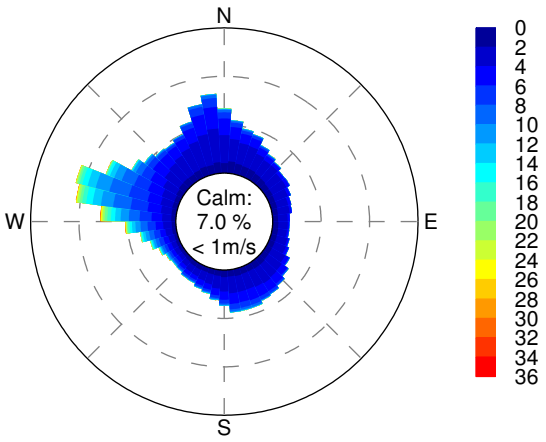

Figure 3. Frequency and speed of valid measurements of winds at 80 m above ground, from 1/1/1996 through 12/31/2010 on the M2 mast. Data are grouped by direction in 7.2° bins and by wind speed in 2 m/s bins. Color bars show wind speeds in 2 m s^{-1} bins.

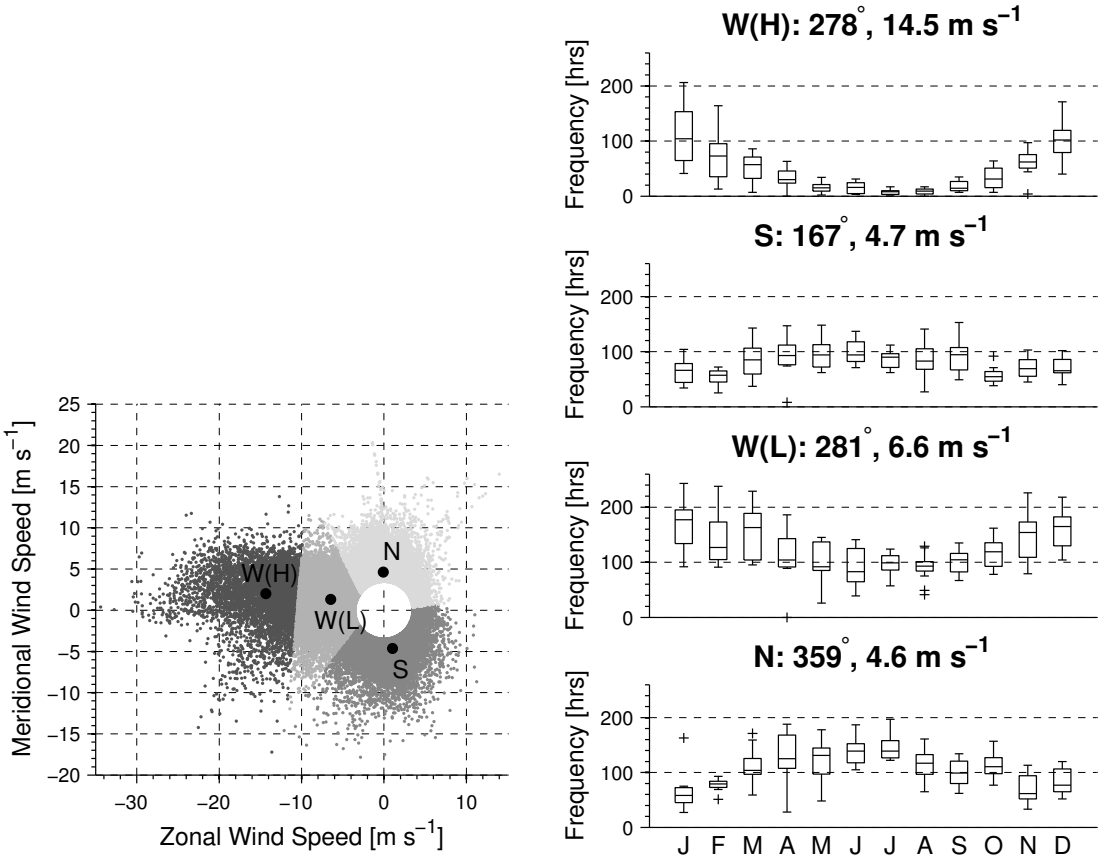

(a) Wind 'clusters' **(b) Monthly cycle of winds.**

Figure 4. Wind clusters at the NWTC. (a) shows the 4 clusters that were identified, and the centroids of those clusters. (b) shows the monthly frequency of winds in each cluster using the same labels as (a). Boxes extend to the 25th and 75th percentiles; whiskers extend to $\pm 2.7\sigma$ or 99.3% of a normal distribution. Outliers are marked with crosses. For details about these plots, see Clifton and Lundquist (2012).

4 Mast design

4.1 Structure

Both the M4 and M5 towers are modified Rohn 80 lattice towers with three cylindrical verticals and double bracing (Figure 5).

- Vertical sections are 3.5 inches (≈0.089 m) external diameter, 41 inches (≈1.04 m) center-to-center.
- Bracing is 1.5-inch angle section.

The mast solidity (the ratio of blocked area to total presented area) is estimated at 0.26 for flows from the prevailing wind direction. This is a relatively high blockage ratio compared to towers that are typically used for wind resource assessments (IEC, 2005; Tusch et al., 2011). The high blockage ratio is caused by the dense cross-bracing that is required to stiffen the mast, and reduce torsion and bending.

The towers are oriented so that one face is at 285° (M4) or 278° (M5) to true north. This orientation is required so that booms can be clamped to the face and extended into the prevailing winds. Booms normal to the winds would not be able to withstand the design conditions on site.

4.2 Anchors, guys and torque arms

The towers are guyed to six anchors that are equally distributed in pairs radially around the mast base. The anchors are approximately 158 feet (50 meters) and 263 feet (80 meters) from the base of the towers. Both M4 and M5 are guyed identically.

The guys are connected to large anti-twist frames around the mast - called torque arms - at several heights on the mast (Table 1 and Figure 6). The torque arms are 15-inch channel that are double the face width of the mast and increase the torsional stiffness of the mast.

4.3 Booms

The two types of booms that are used on the towers are shown in Figure 7. These booms are distinguished by their length and the way that instruments are mounted:

- **Short booms** are 12 feet long, 2-inch square section, retractable aluminum booms from Mast Systems, Inc (`http://www.towersystems.com`). Booms are guyed back to the mast at 3 points. These booms are usually used as mounts for cup anemometers, wind vanes, and temperature sensors.

Table 1. Mast guy configuration. Data include the distance to the anchor, height of the guy cable attachment to the towers, and guy cable diameter. M4 and M5 have identical guy anchors and torque arm heights.

Anchor location	Torque arm height (feet)	Guy cable diameter (inches)
Inner (50 m)	77	1/2
	143	1/2
	197	5/8
Outer (80 m)	277	5/8
	357	3/4
	417	3/4

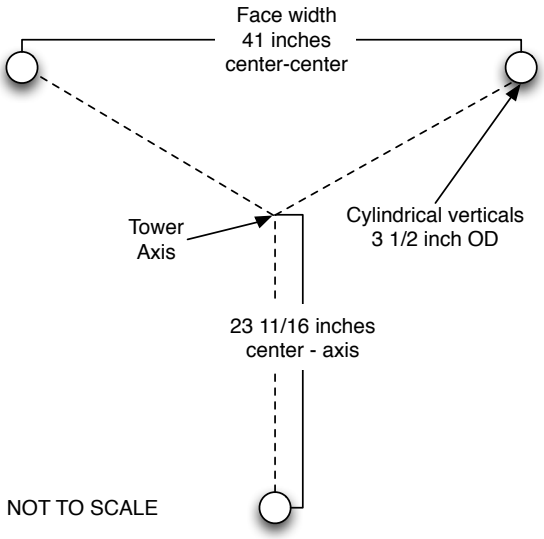

(a) Cross-section of the Rhone-80 lattice mast. Bracing is removed for clarity.

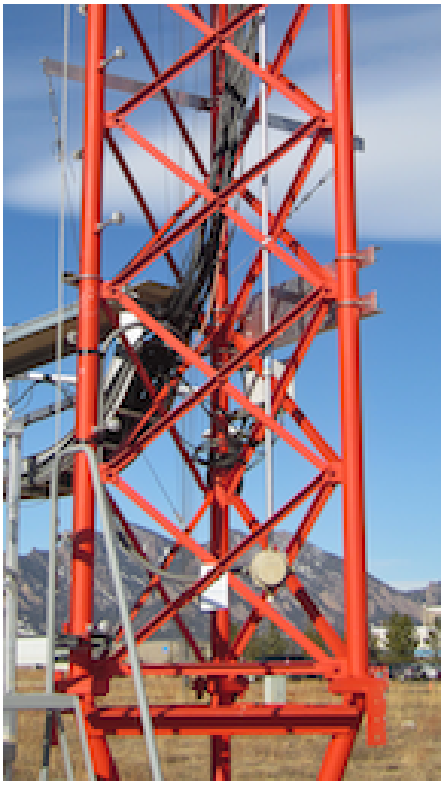

(b) Elevation view of the base of the M5 mast. The 3-m boom is visible above the cable gantry (left). Photo courtesy Lee-Jay Fingersh, NREL.

Figure 5. Mast structure.

Figure 6. Torque arm at 130 m on the M4 mast. The torque arm is the large, triangular frame connected to guy lines leading out of the photograph. The sonic anemometer boom at 131 m a.g.l. is being installed. The cup anemometer and vane at 134 m a.g.l. are also visible. Photo courtesy Lee-Jay Fingersh, NREL.

- **Long booms** were custom designed and built to be extremely rigid when deployed, but also retractable. They are braced on two sides of the mast and guyed above and below. These booms are used only as mounts for the sonic anemometers.

A view from the base of the M4 mast, looking upward, shows the relative lengths of booms on the M4 mast (Figure 8). Some instrumentation can be seen, as well as the orientation of the booms with respect to the guy wires.

4.4 Man lift

A man lift is installed on the outside of the southeast face of the mast. This is a set of cables and 1-inch channel running vertically up the mast. When not in use the man lift is parked at the base of the mast. The man lift does not add to the solidity of the mast.

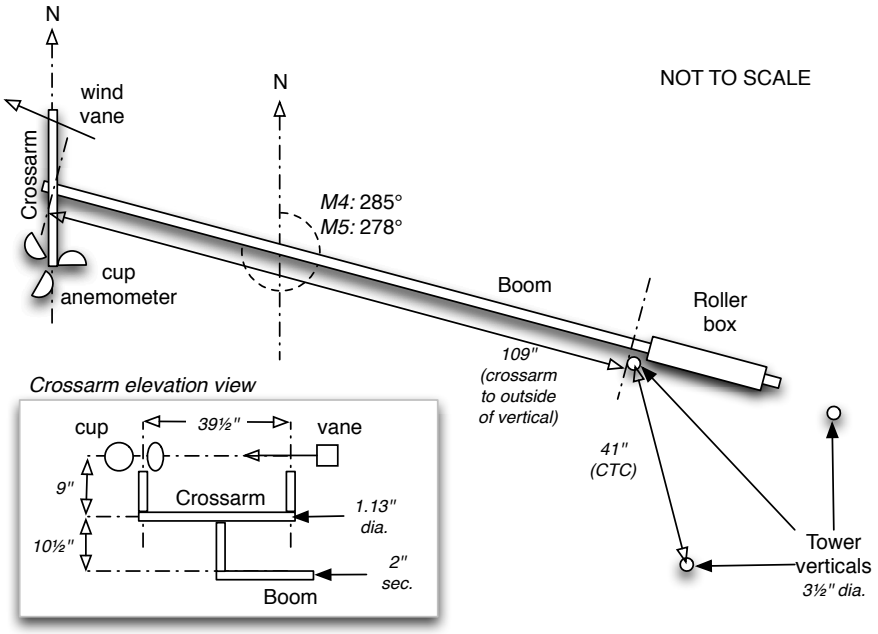

(a) Plan and elevation views of wind direction and wind speed sensors on short booms.

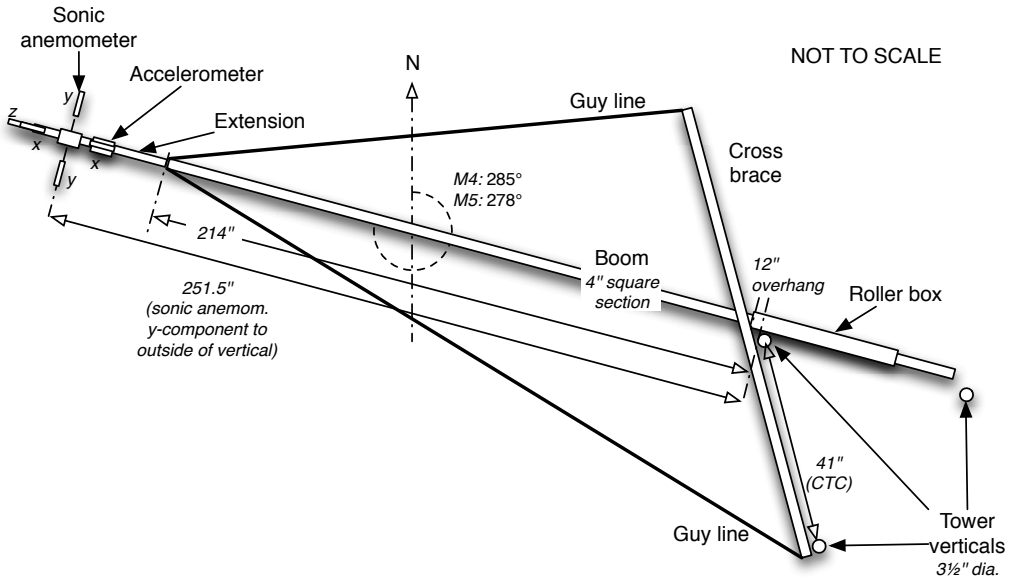

(b) Plan view of sonic anemometers on long booms.

Figure 7. Instrumentation booms on the M4 and M5 towers.

Figure 8. View from the ground of booms and instrumentation on the M4 mast.

5 Instrumentation

Details of the different instruments installed on the M4 and M5 masts are given in Table 2.

Table 2. Devices used to measure atmospheric properties and mast behavior on the M4 and M5 masts. Accuracy data are from the manufacturer's specification sheets unless otherwise stated.

Parameter	Description	Device	Range	Accuracy
WS	Wind speed	Met One SS-201 Cup anem.	0 to 90 m s^{-1}	0.5 m s^{-1} or 2%
$WS(1)$	Wind speed (class one)	Thies 4.3351.10.0000	0 to 75 m s^{-1}	
WD	Wind Direction	Met One SD-201 Vane	0 to 360°	3.6°
T	Air temperature	Met One T-200A platinum RTD	± 50°	
T_{dp}	Dew point temperature	Therm-x 9400ASTD	± 50 °C	
ΔT	Differential temperature	Met One T-200A	-4.44 °C to +6.66 °C	
u_x, u_y, u_z	Wind components	ATI 'K' Type sonic anem.	± 30 m s^{-1}	0.01 m s^{-1}
accn	Boom triaxial acceleration	Summit 34201A	± 2.4g (all axes)	
T_s	Sonic temperature	ATI 'K' Type sonic anem.	-50 °C to +60 °C	0.1°C
P	Barometric pressure	AIR AB-2AX	740 to 1000 mBar	
Precip	Precipitation	Vaisala DRD11A	0 (heavy) to 3 (dry)	None given

5.1 Wind speed and direction measurements

5.1.1 Sonic anemometers

Sonic anemometers calculate the wind speed through a small volume by measuring the difference in the speed of sound in opposite directions through the domain. Applied Technologies 'K' type sonic anemometers are installed on the M4 and M5 masts. These anemometers measure the wind speed in three dimensions (two orthogonal horizontal, one vertical) using three, 15-cm-long open paths. The open path is the gap in the thin 'arms' seen in Figure 9. The theory of operation of sonic anemometers is compared to cup anemometers in Wyngaard (1981). Oncley et al. (1996) gives a comprehensive overview of sonic anemometer data processing.

The sonic anemometers are mounted at the end of long booms. When the booms are extended into position, the sonic anemometers are approximately 251.5 inches' from the outside of the mast leg. This distance is approximately 5.7 times the face width from the mast leg.

A 3-axis accelerometer is installed on the boom near to the sonic anemometer to quantify boom motion (Figure 7 and Figure 9). A copper grounding rod is installed between the arms of the anemometer and connected to a ground wire running down the mast, to provide a route to ground for lighting (Figure 9).

5.1.2 Cup anemometers and wind vanes

Two different types of cup anemometer are used on the M4 and M5 masts (Figure 10). One type is known as a 'class one' or 'first class' anemometer, as the anemometer reaches the highest level of accuracy and repeatability set out in the International Electrotechnical Commission's guidelines for anemometry for power performance testing (IEC, 2005). The class one anemometers used on the M4 and M5 masts are manufactured by Thies (Table 2). Combined cup anemometers and vanes are also installed on the masts. These are Met One wind sensors (model no. WS-201), which are a combination of the Met One cup anemometer (model no. SS-201) and Met One wind vane (model no. SD-201). The cups and vanes are not heated.

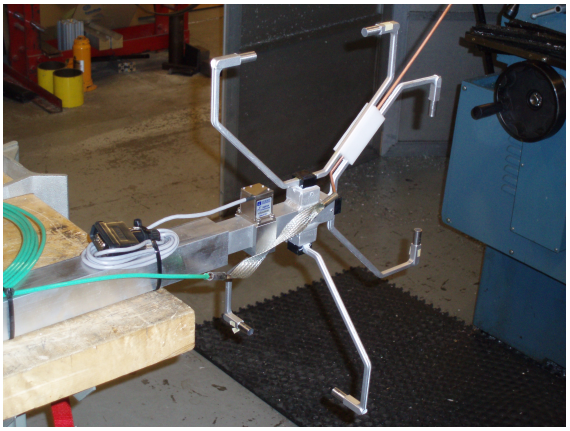

(a) ATI 'K' type sonic anemometer. The x and y wind components are measured with the arms on the top and bottom of the boom. The w wind component is measured with the arm on the end of the boom

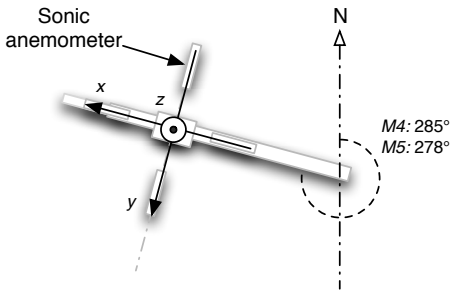

(b) The coordinate system of the 'K- type anemometer when installed on the mast

Figure 9. Sonic anemometers used on the M4 and M5 masts at the NWTC. Compare with Figure 7.

The cups and vanes are mounted at opposite ends of a 1-m crossbar at the end of a 'short' boom (Figure 7). When the booms are extended into position, the Met One cup anemometers and wind vanes are 2.9 m from the nearest mast leg (approximately 2.8 face widths from the mast leg).

5.1.3 Slowing down of flow around the tower

The IEC standard for power performance testing of wind turbines describes how wind speed measurements obtained by cup anemometers on lattice masts might be impacted by the mast structure (Annex G of IEC, 2005). This calculation is performed by assuming that the mast imparts a thrust on the wind in the region of the mast. According to calculations based on the standard that were carried out by an independent inspector, the mast solidity is 0.26, implying a thrust coefficient of the mast of $C_T = 0.4$ if Annex G is followed (Sadoud, 2012). However, based on the inspector's experience, they suggest that the standard underestimates the thrust at this solidity, and suggest increasing it by a factor 2 so that $C_T = 0.8$. The thrust varies with with the direction of flow, and C_T is assumed to be constant with free-stream wind speed. This allows an estimate for the slow down compared to the free stream as a function of wind direction.

The study showed that the maximum reduction in measured wind speed is when flows are directly toward the booms. In the case of winds flowing directly toward the booms:

- The cup anemometers on short booms measure approximately 98% of the free stream wind, and
- The sonic anemometers on long booms measure greater than 99% of the free stream wind.

The wind speed measured by the cup and sonic anemometers is the same as the free stream wind speed when the flows are perpendicular to the booms.

NB: Output wind speeds are not corrected to the free stream wind speed before being saved to file. This is because the effect of the mast structure has not been proven at this time.

The implications of the study are:

- The cups and vanes on short booms are considered secondary windspeed sensors, regardless of their accuracy under calibration.

(a) Thies "First Class" anemometer **(b) Met One anemometer**

Figure 10. Cup anemometers used on the M4 and M5 masts at the NWTC.

- The sonic anemometers (which are mounted on long booms) are the primary windspeed sensors on the masts.

NB: Users are advised to consider the possible impact of the mast structure as a source of uncertainty in the cup wind speeds and values that are derived from it.

5.2 Temperature measurements

The air temperature and dew point temperature measurements are housed together in an aspirated (ventilated) thermal radiation shield. This radiation shield is a Met One 327C (see Figure 11). The air temperature and differential temperature sensors are co-located in the radiation shield, while the dew point sensor is in a separate 'can' in the tube (DP200B, as shown in Figure 11). When the aspirator operates, a flap in the tube is forced open by the air flow and a microswitch is switched. The status of the aspirators is checked and stored in the output data.

Temperature measurements and wind sensors are often co-located on the same short boom. An example of this is on the M4 mast at 3 m, as shown in Figure 12.

Differential temperature measurements are made by subtracting the temperature signal at one height, from the temperature signal at another. This small signal is then amplified and converted to engineering units. This gives a higher accuracy to the temperature difference than would be possible using the difference in the engineering units, alone.

5.3 Barometric pressure

Barometric pressure is measured with a sensor housed in the data collection building near the base of the meteorological masts. The sensors are AIR AB-2AX and are connected to a pressure tap outside the building, 3 m above ground. Pressure sensors are calibrated in the range 780 - 840 mBar, which exceeds the expected range of barometric pressure at this altitude above sea level.

5.4 Precipitation

Precipitation is measured using a precipitation sensor mounted at the data shed, approximately 100 m from the base of the mast. The sensor is a Vaisala DRD11A, which responds to rain and snow. It may also respond to hail. The sensor quantifies precipitation in the range [0-3], with 0 meaning heavy precipitation and 3, no precipitation.

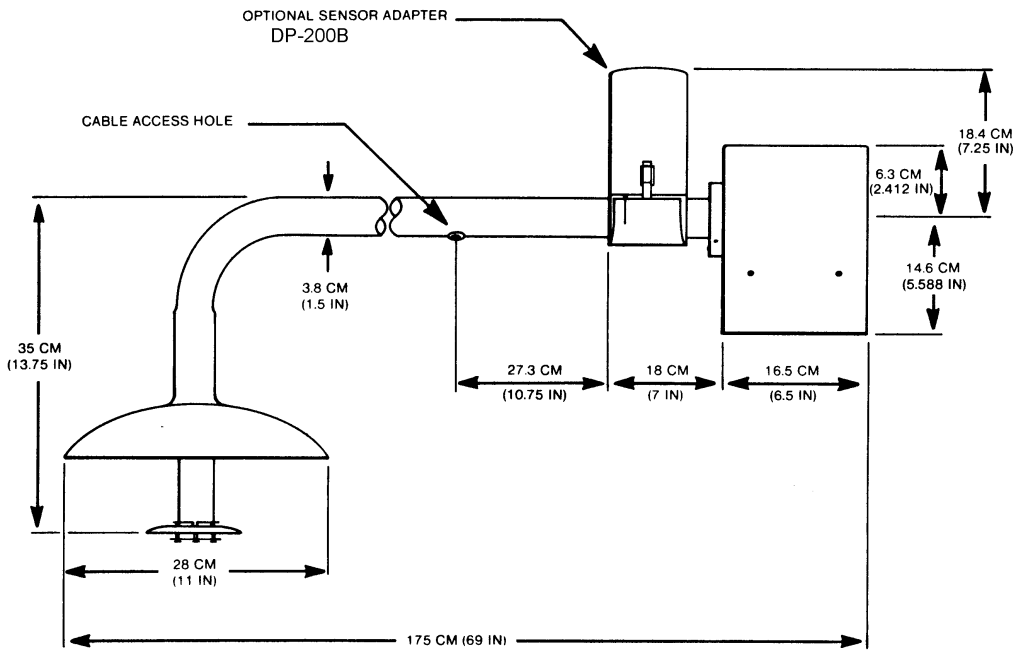

Figure 11. Met One 327C aspirated thermal radiation shield. © Met One Instruments. Used with permission.

5.5 M4 Mast Instrumentation

The M4 mast (also known as the 'site 4.4' or 'Siemens' mast) is 2.5 rotor diameters away from a Siemens 2.3 MW wind turbine (see Figure 2). A sketch of the mast design is shown in Figure 13a. Sensors are listed in Table 3 and described in Table 2.

5.6 M5 Mast Instrumentation

The M5 mast (also known as the 'site 4.4' or 'GE' mast) is 2.5 rotor diameters away from a GE SLE 1.5 MW wind turbine (Figure 2). Instrumentation types and heights on the M5 mast are listed in Table 4. The M5 equipment is similar to the M4 mast instrumentation and is described in Table 2.

Figure 12. Co-located wind sensor WS-201 and aspirated thermal radiation shield M0327C at 3 m above ground on the M4 mast. Author's own photograph.

Table 3. Heights of instrumentation on the M4 mast. Parameters are described in more detail in Table 2.

Height	Parameter	Boom
134	WD, WS, T_{dp}, ΔT	Short
131	u_x, u_y, u_z, T_s, accn	Long
100	u_x, u_y, u_z, T_s, accn	Long
88	WD, WS, T, T_{dp}, ΔT	Short
80	$WS(1)$	Short
76	u_x, u_y, u_z, T_s, accn	Long
50	u_x, u_y, u_z, T_s, accn	Long
30	u_x, u_y, u_z, T_s, accn	Long
26	WD, WS, T, T_{dp}, ΔT	Short
15	u_x, u_y, u_z, T_s, accn	Long
10	WD, WS	Short
3	WD, WS, T, T_{dp}	Short
3	P, precip	N/A

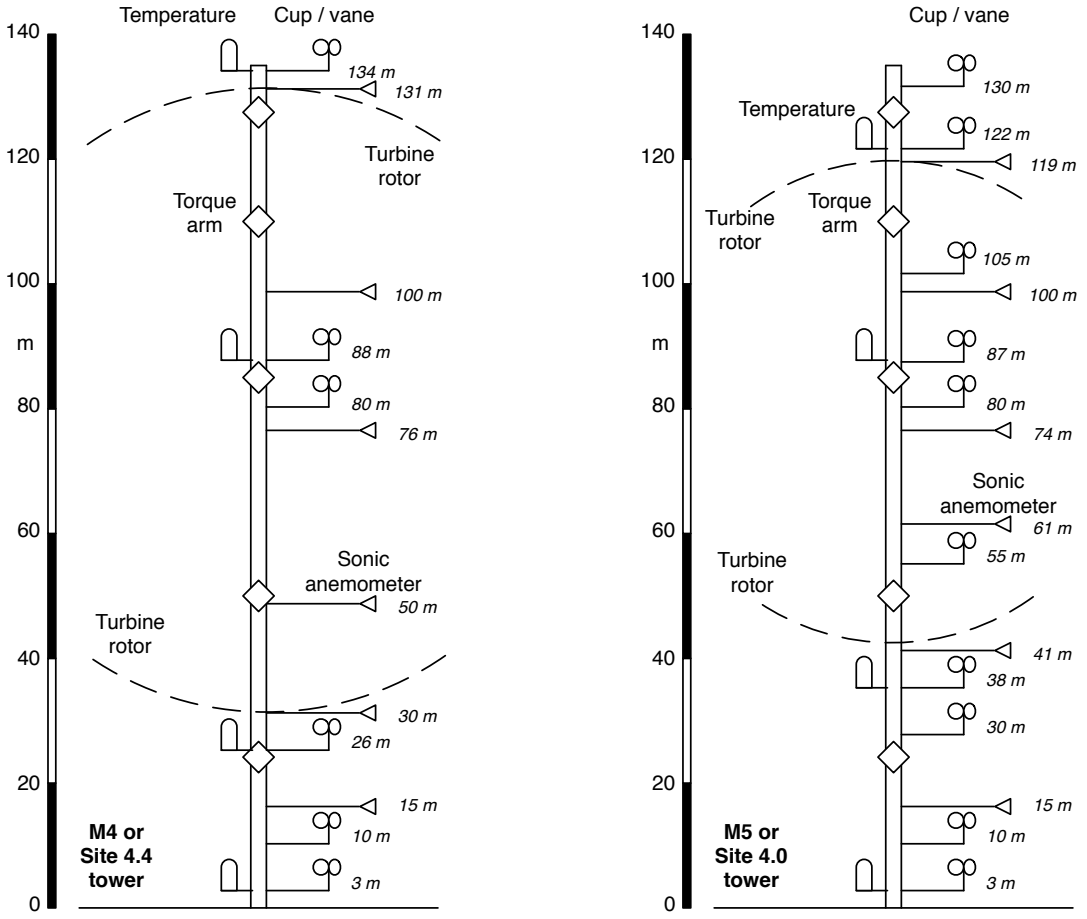

(a) The M4 mast. All booms face 285°.

(b) The M5 mast. All booms face 278°.

Figure 13. Schematic view of the NWTC M4 and M5 masts. Sketch heights are approximate. Height labels are exact.

Table 4. Heights of instrumentation on the M5 mast. Parameters are described in more detail in Table 2.

Height	Parameter	Boom
130	$WS(1)$	Short
122	WD, WS, T_{dp}, ΔT	Short
119	Sonic u_x, u_y, u_z, T_s, accn	Long
105	$WS(1)$	Short
100	Sonic u_x, u_y, u_z, T_s, accn	Long
92	–	Short
90	–	Short
87	WD, WS, T,T_{dp}, ΔT	Short
80	$WS(1)$	Short
74	Sonic u_x, u_y, u_z, T_s, accn	Long
61	Sonic u_x, u_y, u_z, T_s, accn	Long
55	$WS(1)$	Short
41	Sonic u_x, u_y, u_z, T_s, accn	Long
38	WD, WS, T, T_{dp}, ΔT	Short
30	$WS(1)$	Short
15	Sonic u_x, u_y, u_z, T_s, accn	Long
10	WD, WS	Short
3	WD, WS, T, T_{dp}	Short
3	P, precip	N/A

6 Data Acquisition

Data are acquired from the instruments on each mast using a rack-mounted data acquisition system (DAQ). The DAQ system measures voltages, frequencies, and reads serial signals from the equipment on the mast. The signals are converted into engineering units by the software, converted into binary format, and written to 10-minute-long files.

6.1 Hardware

Data acquisition hardware is mounted in 19-inch racks in the data sheds at the NWTC 4.4 and 4.0 sites. The systems are connected to a National Instruments (NI) chassis housing a PC and PXI cards. The PXI cards acquire the signals and transmit the data to the PC, and provide specific functionality. The hardware installed in the data sheds is listed in Table 5.

6.2 Calibration

NREL is accredited by the American Association for Laboratory Accreditation (A2LA) as a wind turbine testing and certification laboratory. This requires certain steps and process to ensure the quality of data that are used. The systems used on the 135-m meteorological masts reflect those requirements, in that every device installed on the masts is documented, calibrated before installation, and recalibrated as required.

6.3 Software

Data is acquired from the PXI chassis by an industrial PC running LabVIEW. The LabVIEW DAQ software creates 10-minute binary data files containing unprocessed 20 Hz data. Data acquisition rates are controlled using a GPS clock, which is also used to generate the timestamp for each 20-Hz data record.

During the data acquisition process, the following happens;

1. Channel definitions are read from the LabVIEW configuration file.
2. A 20 Hz trigger signal is generated by LabVIEW from the GPS timing unit.
3. Every time a 20 Hz timing signal is received;
    - The time is recorded
    - All analog channels, including cups, vanes, and temperatures, are measured
    - Sonic anemometers are triggered and the serial buffer is emptied (there is an approximately 50 ms delay between triggering the sonic anemometer and data being written to the serial buffer).
    - All data are written to file.

Table 5. DAQ hardware. Model numbers are for National Instruments hardware.

Function	Model	Description
Controller	PXI 8108	Embedded PC
GPS timing signal	PXI 6682H	Receive, interpret and rebroadcast GPS time stamp
Serial interface	PXI 8431	Serial ports for communications with sonic anemometers
Analog IO	PXI 6225	Analog signals, e.g. wind directions from vanes
Digital IO	PXI 6624	Status of aspirator fans
Pulse counting	PXI 6624	Pulse counting (e.g. cup anemometers)

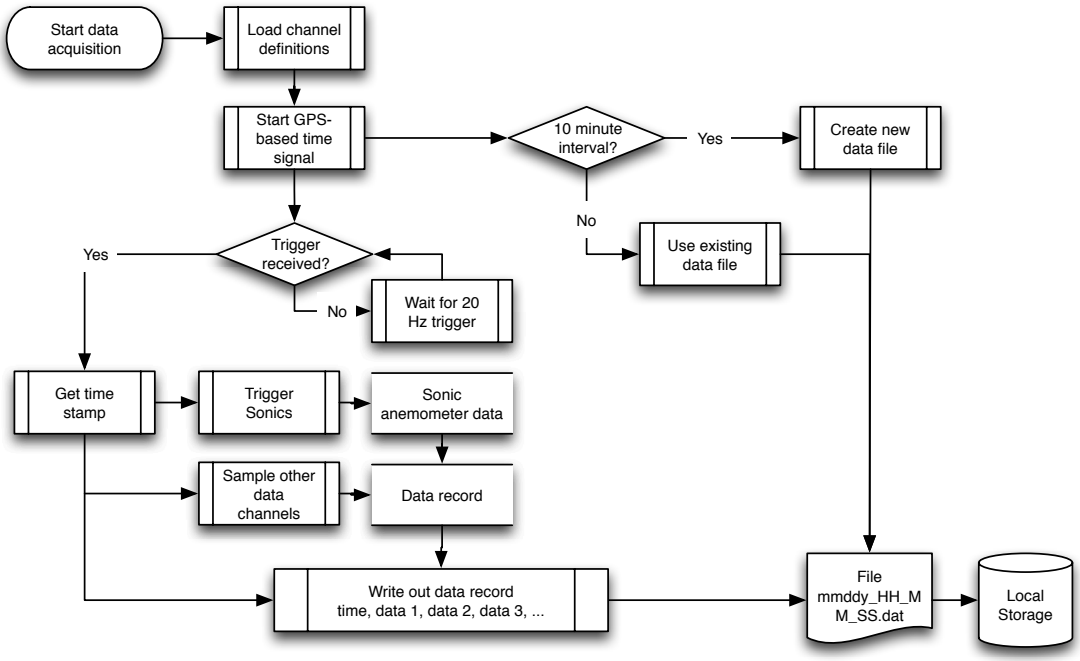

Figure 14. Data acquisition process.

4. Every 10 minutes, a new data file is started.

This process is summarized in Figure 14.

6.3.1 Inline data processing

All data are acquired as voltage, frequency or digital signals. Those raw signals are converted as appropriate into engineering units (e.g. m s^{-1}, °C) using calibrated transfer functions. Instantaneous wind directions (WD) greater than 360°are mapped to (WD-360). Values less than 0 are mapped to (WD+360). The presence of wind directions less than or greater than 360° can occur as a result of the calibration of the vane to local north. Other data are written out to file in engineering units with no checking or modification.

6.3.2 Raw data files

Data are written to binary files that contain ten minutes of raw data. A new file is started every 10 minutes at HH:00, HH:10, HH:20, etc. Data are scaled from floating point values to integer values before being written to the binary file.

6.4 Operations Metadata

Limited observational metadata are stored in a database system which is only available from within the NREL local area network, to authorized users. Examples of metadata stored in the system include system outages, known instrument failures or system modifications. These data are available on request.

Outage information is also stored in a machine-readable 'outage' file that is updated by hand as outages are identified. The outage file is queried every time a new 10-minute data file is analyzed. If outages are identified for a channel or group of channels, those data are set to *NaN* for the period of the outage. Data known to be 'bad' or questionable are therefore removed from the processed data, but still available in the raw data.

7 Data Processing

The following sections describe how measured values are converted into 10-minute values and combined to calculate other properties. Where possible, data processing follows the same methods as used at the NWTC for the M2 mast.

Data processing follows a step-by-step process:

1. Instrument data are read from archived, raw binary data files. These are 10-minute files of 20 Hz data.
2. Data are quality controlled. First, metadata are queried, and potentially 'bad' data are marked. Then, data from each instrument channel are checked against manufacturers' limits and 'normal' operating limits.
3. Means and standard deviations are calculated for each channel.
4. Data from the sonic anemometers are analyzed.
5. Data from more than one channel are combined into relevant parameters, called 'derived values'.
6. Results of data processing and quality controlled are stored together with other information about time of acquisition, descriptive text and units. These are individual files that describe the average conditions during the 10-minute interval.

The routines described above are implemented in MATLAB r2010b.

7.1 Raw time series data from individual sensors

The 10-minute long, 20-Hz binary data file that was written out by the data acquisition system is unpacked and read into MATLAB.

7.1.1 Data channels on the M4 mast

The instrumentation that was shown in Figure 3 generates approximately 65 data channels, listed in Table 6. Channel numbers are equivalent to the column number of the data in the 10-minute data file that was written out by the mast DAQ. In some cases, one instrument can generate multiple channels. Examples of this include the sonic anemometers, which generate data streams for each of three wind components and a temperature.

Table 6. M4 data channels. See also Table 3.

Channel	Description	Variable	height
6	Sonic x velocity	Raw_Sonic_x_131	131
7	Sonic y velocity	Raw_Sonic_y_131	131
8	Sonic z velocity	Raw_Sonic_z_131	131
9	Sonic temperature	Raw_Sonic_Temp_131	131
10	Sonic x velocity	Raw_Sonic_x_100	100
11	Sonic y velocity	Raw_Sonic_y_100	100
12	Sonic z velocity	Raw_Sonic_z_100	100
13	Sonic temperature	Raw_Sonic_Temp_100	100
14	Sonic x velocity	Raw_Sonic_x_76	76
15	Sonic y velocity	Raw_Sonic_y_76	76
16	Sonic z velocity	Raw_Sonic_z_76	76
17	Sonic temperature	Raw_Sonic_Temp_76	76
18	Sonic x velocity	Raw_Sonic_x_50	50
19	Sonic y velocity	Raw_Sonic_y_50	50

Channel	Description	Variable	height
20	Sonic z velocity	Raw_Sonic_z_50	50
21	Sonic Temperature	Raw_Sonic_Temp_50	50
22	Sonic x velocity	Raw_Sonic_x_30	30
23	Sonic y velocity	Raw_Sonic_y_30	30
24	Sonic z velocity	Raw_Sonic_z_30	30
25	Sonic temperature	Raw_Sonic_temp_30	30
26	Sonic x velocity	Raw_Sonic_x_15	15
27	Sonic y velocity	Raw_Sonic_y_15	15
28	Sonic z velocity	Raw_Sonic_z_15	15
29	Sonic temperature	Raw_Sonic_Temp_15	15
30	Air temperature	Raw_Air_Temp_88m	88
31	Air temperature	Raw_Air_Temp_26m	26
32	Air temperature	Raw_Air_Temp_3m	3
33	Dewpoint temperature	Raw_Dewpt_Temp_134m	134
34	Dewpoint temperature	Raw_Dewpt_Temp_88m	88
35	Dewpoint temperature	Raw_Dewpt_Temp_26m	26
36	Dewpoint temperature	Raw_Dewpt_Temp_3m	3
37	Δ T	Raw_DeltaT_134_88m	134
38	Δ T	Raw_DeltaT_88_26m	26
39	Δ T	Raw_DeltaT_26_3m	3
40	Vane wind direction	Raw_Vane_WD_134m	134
41	Vane wind direction	Raw_Vane_WD_88m	88
42	Vane wind direction	Raw_Vane_WD_26m	26
43	Vane wind direction	Raw_Vane_WD_10m	10
44	Vane wind direction	Raw_Vane_WD_3m	3
45	Acceleration in x	Raw_Accel_x_131	131
46	Acceleration in y	Raw_Accel_y_131	131
47	Acceleration in z	Raw_Accel_z_131	131
48	Acceleration in x	Raw_Accel_x_100	100
49	Acceleration in y	Raw_Accel_y_100	100
50	Acceleration in z	Raw_Accel_z_100	100
51	Acceleration in x	Raw_Accel_x_76	76
52	Acceleration in y	Raw_Accel_y_76	76
53	Acceleration in z	Raw_Accel_z_76	76
54	Acceleration in x	Raw_Accel_x_50	50
55	Acceleration in y	Raw_Accel_y_50	50
56	Acceleration in z	Raw_Accel_z_50	50
57	Acceleration in x	Raw_Accel_x_30	30
58	Acceleration in y	Raw_Accel_y_30	30
59	Acceleration in z	Raw_Accel_z_30	30
60	Acceleration in x	Raw_Accel_x_15	15
61	Acceleration in y	Raw_Accel_y_15	15
62	Acceleration in z	Raw_Accel_z_15	15
63	Station Pressure	Raw_Baro_Presr_3m	3
64	Precipitation intensity	Raw_PRECIP_INTEN	0
65	Cup wind speed	Raw_Cup_WS_134m	134
66	Cup wind speed	Raw_Cup_WS_88m	88
67	Cup wind speed	Raw_Cup_WS_80m	80
68	Cup wind speed	Raw_Cup_WS_26m	26

Channel	Description	Variable	height
69	Cup wind speed	Raw_Cup_WS_10m	10
70	Cup wind speed	Raw_Cup_WS_3m	3

7.1.2 Data channels on the M5 Mast

Data channels on the M5 Mast (Table 7) are similar to those on the M4 mast (Table 6). Channel names on M5 are slightly different to M4, because of the different instrument heights and instrumentation on M5 compared to M4. Class one anemometers are indicated using the suffix 'C1' in the variable name, before the installation height.

Table 7. M5 data channels. See also Table 4.

Channel	Description	Variable	height
6	Sonic x velocity	Raw_Sonic_x_119	119
7	Sonic y velocity	Raw_Sonic_y_119	119
8	Sonic z velocity	Raw_Sonic_z_119	119
9	Sonic temperature	Raw_Sonic_Temp_119	119
10	Sonic x velocity	Raw_Sonic_x_100	100
11	Sonic y velocity	Raw_Sonic_y_100	100
12	Sonic z velocity	Raw_Sonic_z_100	100
13	Sonic temperature	Raw_Sonic_Temp_100	100
14	Sonic x velocity	Raw_Sonic_x_74	74
15	Sonic y velocity	Raw_Sonic_y_74	74
16	Sonic z velocity	Raw_Sonic_z_74	74
17	Sonic temperature	Raw_Sonic_Temp_74	74
18	Sonic x velocity	Raw_Sonic_x_61	61
19	Sonic y velocity	Raw_Sonic_y_61	61
20	Sonic z velocity	Raw_Sonic_z_61	61
21	Sonic Temperature	Raw_Sonic_Temp_61	61
22	Sonic x velocity	Raw_Sonic_x_41	41
23	Sonic y velocity	Raw_Sonic_y_41	41
24	Sonic z velocity	Raw_Sonic_z_41	41
25	Sonic temperature	Raw_Sonic_temp_41	41
26	Sonic x velocity	Raw_Sonic_x_15	15
27	Sonic y velocity	Raw_Sonic_y_15	15
28	Sonic z velocity	Raw_Sonic_z_15	15
29	Sonic temperature	Raw_Sonic_Temp_15	15
30	Air temperature	Raw_Air_Temp_87m	87
31	Air temperature	Raw_Air_Temp_38m	38
32	Air temperature	Raw_Air_Temp_3m	3
33	Dewpoint temperature	Raw_Dewpt_Temp_122m	122
34	Dewpoint temperature	Raw_Dewpt_Temp_87m	87
35	Dewpoint temperature	Raw_Dewpt_Temp_38m	38
36	Dewpoint temperature	Raw_Dewpt_Temp_3m	3
37	Δ T	Raw_DeltaT_122_87m	122
38	Δ T	Raw_DeltaT_87_38m	38
39	Δ T	Raw_DeltaT_38_3m	3
40	Vane wind direction	Raw_Vane_WD_122m	122
41	Vane wind direction	Raw_Vane_WD_87m	87

Channel	Description	Variable	height
42	Vane wind direction	Raw_Vane_WD_38m	38
43	Vane wind direction	Raw_Vane_WD_10m	10
44	Vane wind direction	Raw_Vane_WD_3m	3
45	Acceleration in x	Raw_Accel_x_119	119
46	Acceleration in y	Raw_Accel_y_119	119
47	Acceleration in z	Raw_Accel_z_119	119
48	Acceleration in x	Raw_Accel_x_100	100
49	Acceleration in y	Raw_Accel_y_100	100
50	Acceleration in z	Raw_Accel_z_100	100
51	Acceleration in x	Raw_Accel_x_74	74
52	Acceleration in y	Raw_Accel_y_74	74
53	Acceleration in z	Raw_Accel_z_74	74
54	Acceleration in x	Raw_Accel_x_61	61
55	Acceleration in y	Raw_Accel_y_61	61
56	Acceleration in z	Raw_Accel_z_61	61
57	Acceleration in x	Raw_Accel_x_41	41
58	Acceleration in y	Raw_Accel_y_41	41
59	Acceleration in z	Raw_Accel_z_41	41
60	Acceleration in x	Raw_Accel_x_15	15
61	Acceleration in y	Raw_Accel_y_15	15
62	Acceleration in z	Raw_Accel_z_15	15
63	Station Pressure	Raw_Baro_Presr_3m	3
64	Precipitation intensity	Raw_PRECIP_INTEN	0
65	Cup wind speed	Raw_Cup_WS_C1_130m	130
66	Cup wind speed	Raw_Cup_WS_122m	122
67	Cup wind speed	Raw_Cup_WS_C1_105m	105
68	Cup wind speed	Raw_Cup_WS_87m	87
69	Cup wind speed	Raw_Cup_WS_C1_80m	80
70	Cup wind speed	Raw_Cup_WS_C1_55m	55
71	Cup wind speed	Raw_Cup_WS_38m	38
72	Cup wind speed	Raw_Cup_WS_C1_30m	30
73	Cup wind speed	Raw_Cup_WS_10m	10
74	Cup wind speed	Raw_Cup_WS_3m	3

7.2 Raw data quality control

Quality control is a rules-based process that is used to remove bad data from the raw time series data.

7.2.1 Checking against limits

The first stage of data cleaning is to check that data is within limits. This data processing is carried out for all 20-Hz data from each channel, against limits that are defined in the configuration files. Two limits are defined:

1. **Manufacturers' stated limits.** These are taken from the specification sheets for the instrumentation. For example, a temperature sensor on channel 30 may have a range of ± 50 °C. These limits correspond to the ranges listed in Table 2.
2. **Users' stated limits.** These are the user's own limits and might be adjusted to account for the DAQ system capability. For example, a temperature sensor may have user-defined limits of ± 49.9 °C, which may correspond

to a signal within the limits of the data acquisition system (say, $\pm$ 5 V). If those limits are met or exceeded, this implies that the measurement is at the limits of the DAQ system's capability and may be erroneous.

High-frequency data that exceed the manufacturers' or users' limits are replaced with *NaN*.

7.2.2 Encoding data quality

Results of quality control are recorded using numerical quality-control (QC) codes. The quality-control codes are recorded in the output data structure for each channel.

- If no quality code is recorded, data are considered to have passed the automated quality control process.
- Data channels are 'flagged' if data quality is reduced but data may still be useful. Reasons for flagging could include:
  - **Irregular timing.** The period between measurements should be 0.05 seconds at a data acquisition rate of 20 Hz. If more than 1% of data are more than 5% from the ideal period, a quality-control code is set.
  - **Data rates** If the number of points within the manufacturer's limits or users' limits is below a threshold set in the configuration file, a quality-control code is set.
  - **Low standard deviation.** If the standard deviation drops below 0.01% of the mean, a channel is assumed to have a constant value during the measurement interval and a quality-control code is set.
- Data channels 'fail' if data are considered definitely unusable. Reasons for failing data include:
  - **Empty data channel.** If a channel is empty, a quality-control code is set.
  - **All bad values.** If all data in a channel have known 'bad' values, e.g. -999, a quality-control code is set.
  - **All *NaN*s.** If all data in a channel are not-a-number (*NaN*), a quality-control code is set.
- Other quality-control codes may also be added during the data processing. These are detailed in the next pages.

7.2.3 Cascading Flags and Fails

In the event that an error is detected in data from one instrument, another instrument can be flagged or failed. For example, all of the channels of a sonic anemometer (3 velocities and one temperature) could be linked together. The process is iterative, in that a failure in one instrument will be cascaded to another, and then another, as defined in the configuration file.

7.3 10-minute means and standard deviations

The mean and standard deviation of the data measured by each channel have many uses. For example, they can be used to identify potentially interesting subsets of the mast data.

7.3.1 Mean values

The arithmetic mean of data from each of the channels listed in Table 6 is the mean of all valid measurements during the 10-minute interval. It is calculated using the MATLAB function `nanmean`.

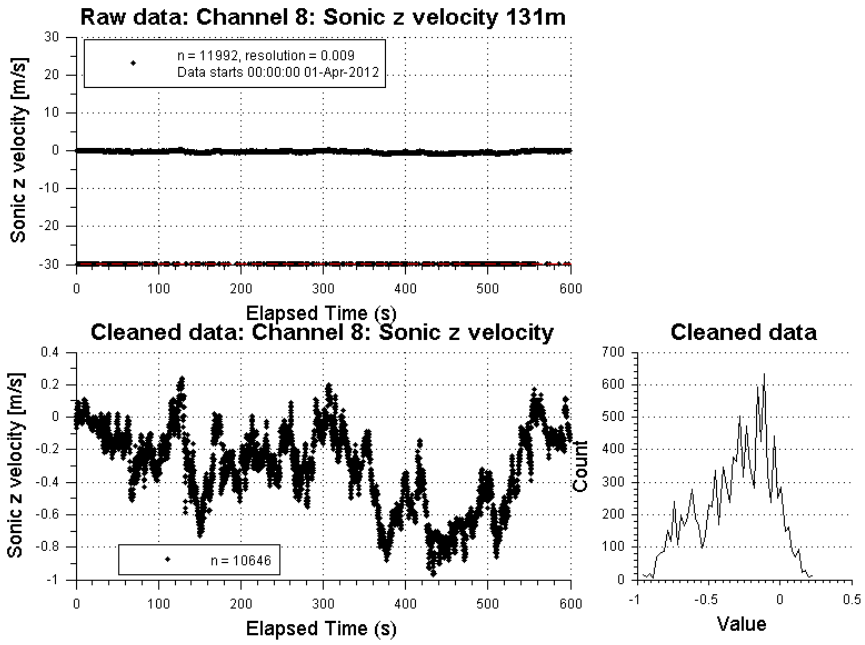

(a) Sonic anemometer. Several data points are found at the lower limit.

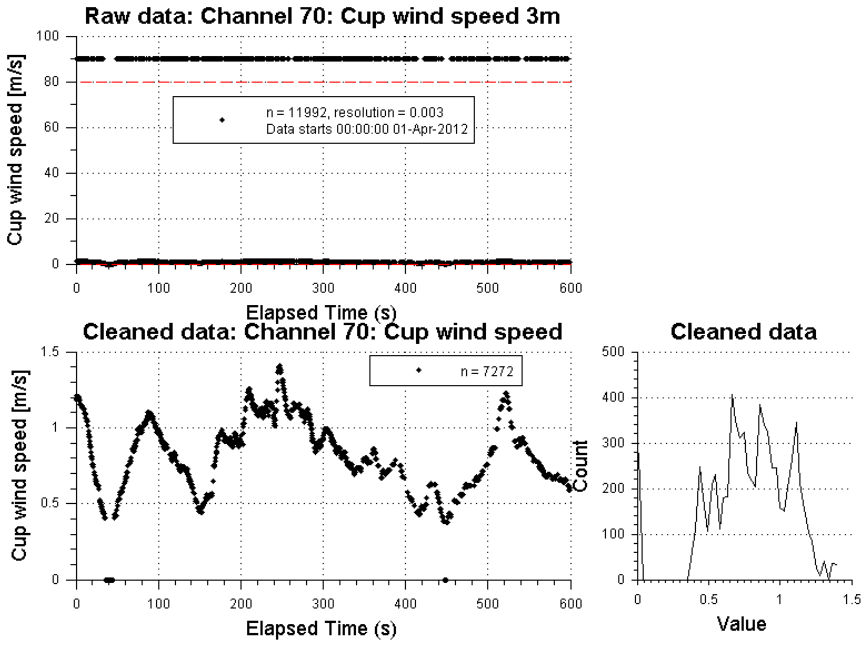

(b) Cup anemometer. Several data points are found at the lower limit.

Figure 15. Example of cleaning data to remove data outside limits.

7.3.2 Standard deviations

The standard deviation of data from each of the channels listed in Table 6 is the standard deviation of all valid measurements during the 10-minute interval. It is calculated using the MATLAB function `nansdev`.

7.4 Cup anemometer data

7.4.1 Mean Wind Speed (cups)

Wind speed is measured at 20 Hz using cup anemometers. A cup anemometer measures the magnitude of the horizontal wind vector to give a time series, u_{cup}. The mean wind speed U_{cup} is simply the arithmetic mean of all measured wind speeds:

$$U_{cup} = \overline{u_{cup}}. \tag{7.1}$$

7.4.2 Turbulence Intensity (cups)

The turbulence intensity measured by the cup is the standard deviation of the instantaneous wind speed measured during a 10-minute interval ($\sigma(u)$), divided by the mean wind speed in a 10-minute interval (U_{cup}):

$$Ti_{cup} = 100 \times \frac{\sigma(u_{cup})}{U_{cup}}. \tag{7.2}$$

Output data: Ti for anemometers at different heights.

7.5 Sonic anemometer data

The sonic anemometers measure wind speed in 3 directions (denoted u_x, u_y and u_z) and a sonic temperature derived from the speed of sound, T_s. The following section describes the data that are derived from a single sonic anemometer at one height.

Figure 16 shows the steps involved in the processing of the sonic anemometer data.

Sonic data are given quality-control codes that summarize the performance of different components in the data chain:

- System timing. Timing requirements are the same as other data channels (see Section 7.2.2). If more than 1% of intervals between data are more than 5% from the target, a quality-control code is set.
- Boom motion. If the maximum detected boom speed exceeds 0.1 m/s at any time during the 10 minute interval, a quality-control code is set.
- Sonic channels. If any of the individual sonic velocity component channels or temperature channel are quality-control coded indicating low standard deviation, an empty data channel, all bad values, or all NaNs, these quality codes are inherited. Other quality codes are ignored.

The sonic coordinate system is shown in Figure 9.

7.5.1 De-noising

Sonic anemometer data can be filtered to remove spikes from the raw wind components and temperature data. Spikes are defined as statistically unlikely departures from the time series that last only for a single measurement. In this application, spikes are detected where the change in u_x, u_y or u_z from one measurement to the next is in the top or bottom 1% of all changes, and is immediately followed by a change of the opposite direction that is also in the top

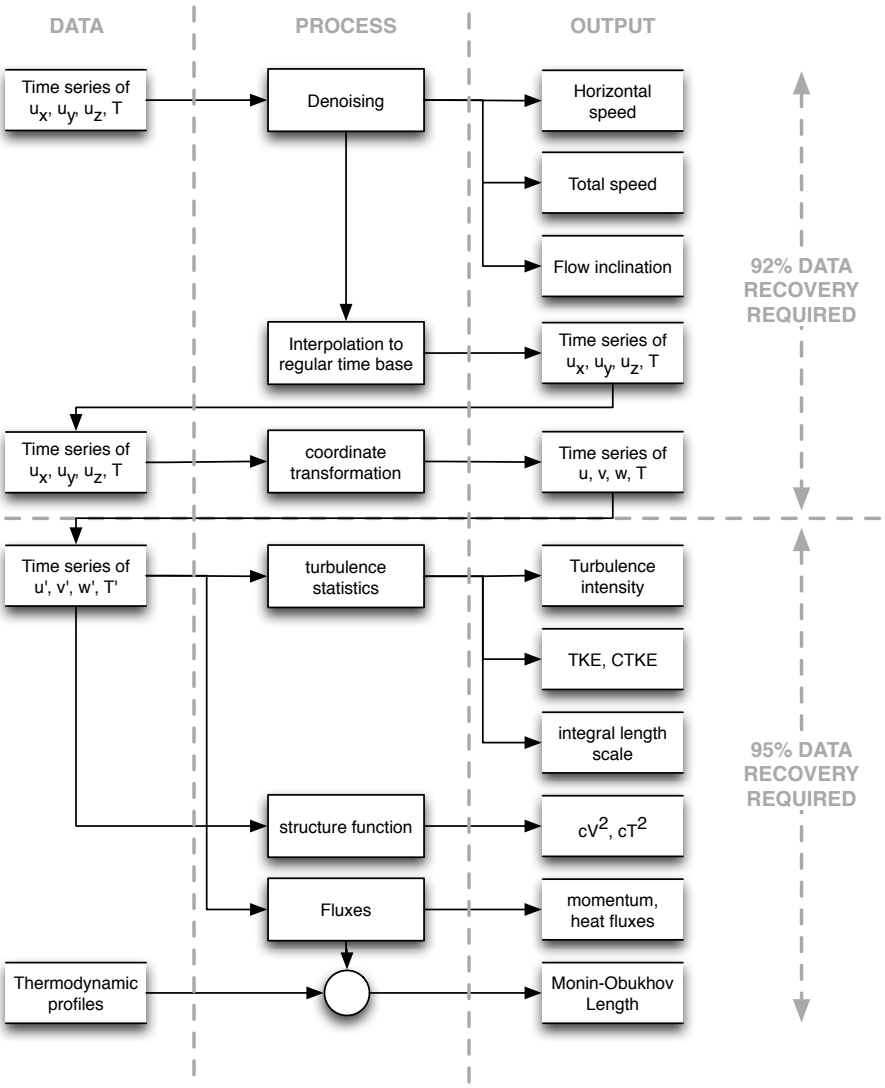

Figure 16. Steps in sonic data processing.

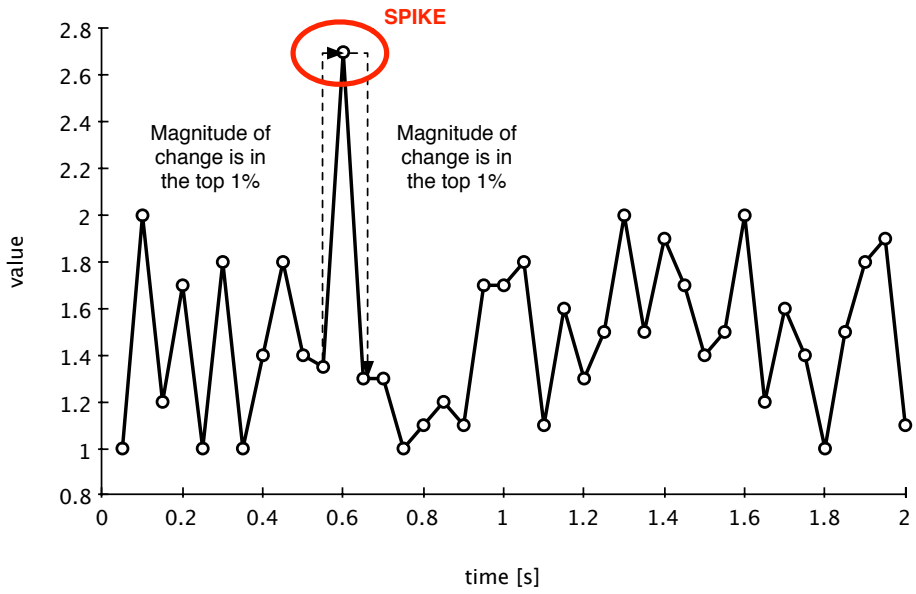

Figure 17. Illustration of spike detection. A high-magnitude change in one direction is followed by another high magnitude change. The outlying measurement is marked as a spike.

1% of all changes (Figure 17). Detected spikes are then replaced with *NaN*s in the time series of temperature and the velocity components.

De-noising is applied for all intervals where the percentage of good data exceeds a threshold level (95%). A text string detailing the number of spikes found is written to the log file. No data are output to the results file.

7.5.2 Horizontal speed

The horizontal wind speed u_H is defined as the resultant of the horizontal wind components u_x and u_y measured by the sonic anemometer. This calculation assumes that the sonic anemometers were installed horizontal with respect to the local gravitational field.

The instantaneous horizontal wind speed (u_H) is defined as

$$u_H = \sqrt{u_x^2 + u_y^2} \tag{7.3}$$

The mean horizontal wind speed for an interval (U_H) is defined as

$$U_H = \left[\overline{u_x}^2 + \overline{u_y}^2\right]^2 \tag{7.4}$$

Horizontal wind speeds are calculated for all intervals where the percentage of good data exceeds a threshold value (92%).

Output data: horizontal wind speed from sonic anemometers at different heights, $U_H(z)$.

7.5.3 Cup-equivalent mean wind speed

The cup-equivalent mean wind speed U_{CupEq} is the time-average of the instantaneous horizontal wind speeds. It is defined as:

$$U_{CupEq} = \overline{u_H} \tag{7.5}$$

Output data: cup-equivalent wind speed from sonic anemometers at different heights, $U_{CupEq}(z)$.

7.5.4 Cup-equivalent turbulence intensity

A cup-equivalent turbulence intensity Ti_{CupEq} is calculated from the time series of the horizontal wind speeds and the cup-equivalent mean wind speed. It is defined as

$$Ti_{CupEq} = 100 \times \frac{\sigma(u_H)}{U_{CupEq}} [\%] \tag{7.6}$$

Output data: cup-equivalent turbulence intensity from sonic anemometers at different heights, $Ti_{CupEq}(z)$.

7.5.5 Total wind speed

The mean total wind speed U_{Total} is defined as the vector-average of the mean de-noised horizontal wind components u_x, u_y and u_z measured by the sonic anemometer. This calculation assumes that the sonic anemometers were installed horizontal with respect to the local gravitational field.

The total wind speed for an interval is defined as

$$U_{Total} = \left[\overline{u_x}^2 + \overline{u_y}^2 + \overline{u_z}^2\right]^{1/2} \tag{7.7}$$

Total wind speeds are calculated for all intervals where the percentage of good data exceeds a threshold value (92%).

Output data: total wind speed from sonic anemometers at different heights, $U_{Total}(z)$.

7.5.6 Inflow angle

The inflow angle β is defined as the angle from the horizontal of the resultant between the time-averaged vertical wind speed and the mean horizontal wind speed:

$$\beta = \arctan\left(\frac{\overline{u_z}}{U_H}\right) \tag{7.8}$$

This calculation assumes that the sonic anemometers were installed horizontal with respect to the local gravitational field.

Output data: inflow angle (degrees from horizontal) from sonic anemometers at different heights, $\beta(z)$.

7.5.7 Remapping to regular time base

De-noised velocity component and temperature data are linearly re-mapped from the measured time base to an ideal 20-Hz time base. This step is required to generate an evenly sampled time series for the calculations described in the following sections.

The remapping involves the following steps, and is performed for each of the velocity components and the temperature data acquired from the sonic anemometers:

1. Generate an empty 20-Hz time series.
2. Populate the empty 20-Hz time series by finding the nearest neighbors from the original time series. Each measurement can only be used for one point in the new time series.
3. Fill gaps in the new data using linear interpolation between data points.
4. If the time series is short (but includes more than 95% of the 10-minute interval), extrapolate the time series to a full ten minutes by appending the mean value of the time series.

NB: this remapping method assumes that the GPS-triggered sampling is carried out at exactly 20 Hz but that there may be occasions in the sampling where the data are not recorded at exactly 0.05-second intervals. These gaps in data acquisition could be caused by problems with instrumentation or high computer CPU loads.

Output data: time series of resampled x, y and z velocities and the temperature from sonic anemometers at different heights. These data are also used in later calculations.

7.5.8 Coordinate transformation (rotation)

The booms on the tall masts are oriented towards the prevailing winds on site, which are approximately northwesterly. Prevailing winds are thus oriented similarly to the x, y, and z axes of the sonic anemometers. In comparison, winds from other directions will pass at an angle through the measurement volume of the sonic anemometers. Rotation is the process of identifying the directional offset of the mean flow from the frame of reference of the anemometer. This offset can be used to convert measured x, y, and z velocities to streamwise, lateral and vertical with respect to the mean flow through the measurement volume.

Data from the 135-m masts are rotated using a 2-axis rotation, which corrects for the pitch and yaw of the sonic with respect to the flow. First, the de-noised and re-mapped data are rotated around the vertical axis so that the mean lateral velocity, $\overline{v} = 0$. Next, the rotated data are rotated around the lateral (v) axis so the mean vertical velocity $\overline{w} = 0$.

NB: coordinate transformation is only used if the number of data points exceeds a threshold value (95%). The calculations described in sections 7.5.9 to 7.5.18 are only made if there are sufficient data points. Otherwise data are set to *NaN* and a quality control code is recorded.

Output data: time series and standard deviations of the streamwise velocity u, lateral velocity v, and vertical velocity w from sonic anemometers at different heights. These data are also used in later calculations.

Source: Weber (1999), Wilczak et al. (2001).

7.5.9 Advection speed

A time-averaged advection speed is defined as the time-average of the streamwise velocity:

$$U_{Ad} = \overline{u} \tag{7.9}$$

7.5.10 Wind speed trend

The wind speed trend is quantified as the gradient of an ordinary least squares fit to the streamwise velocity with respect to time, during the measurement interval.

NB: much of the processing of sonic anemometer or boundary layer data assumes that the boundary layer is stationary during the 10-minute observation interval. If there is a significant rate of change of the wind speed during the observation interval, this assumption of stationarity may be incorrect.

Output data: rate of change of the streamwise velocity from sonic anemometers at different heights.

7.5.11 Turbulent velocity components

The wind speed measured at an instant in time is the sum of the mean and the turbulent components of the wind speed. After rotation into the prevailing wind, this is defined for the streamwise, later and vertical flow, and temperature, as:

$$u(t) = \overline{u} + u' \tag{7.10}$$
$$v(t) = \overline{v} + v' \tag{7.11}$$
$$w(t) = \overline{w} + w' \tag{7.12}$$
$$T_s(t) = \overline{T_s} + T_s' \tag{7.13}$$

The turbulent fluctuation is defined as the difference compared to a fit to the 10-minute time series. For generally stationary flow, the fit is the mean, while for other cases or longer averaging times it may be appropriate to de-trend the data. The turbulent velocity component is only calculated for rotated wind speed data. It is calculated for the streamwise, lateral and vertical components of velocity. The turbulent component of the temperature measured by the sonic anemometer is also calculated.

NB: there is limited agreement in the literature on the correct order of fit to use for de-trending data. Theoretically, any order of fit greater than or equal to 0 could be used, where a zero-order fit would estimate the mean value, and thus turbulence would be defined as the difference compared to the mean. However, the low frequency content of the turbulence decreases as the order of the fit increases. The data processing used at the NWTC assumes a zero-order fit, i.e. that there is no underlying trend in conditions during the 10-minute interval. This can be checked for each 10-minute interval (see Section 7.5.10).

7.5.12 Friction velocity

Friction velocity u_* is a velocity scale for the atmospheric boundary layer (Garratt, 1994; Stull, 1988). In this case, it is calculated from the covariance of the turbulent components of rotated sonic anemometer data:

$$u_* = \left[\overline{u'w'}^2 + \overline{v'w'}^2\right]^{\frac{1}{4}} \tag{7.14}$$

Output data: friction velocity from sonic anemometers at different heights, $u_*(z)$.

Source: Weber (1999).

7.5.13 Convective temperature scale

Sometimes referred to as the friction temperature, the convective temperature scale Θ_* is defined as:

$$\Theta_* = -\frac{\overline{w'\Theta'}}{u_*} \tag{7.15}$$

where u_* is the local friction velocity derived from the sonic anemometer measurements, and Θ' is the potential temperature fluctuation. High frequency measurements of Θ_* are not made. Instead, we assume that fluctuations of the sonic temperature are a good approximation to fluctuations of the potential temperature, so that $T_s' \approx \Theta'$. Therefore we can use:

$$\Theta_* = -\frac{\overline{w'T_s'}}{u_*} \tag{7.16}$$

where w is the vertical velocity component derived from the sonic temperature, Θ is the potential temperature, and u_* is the local friction velocity.

NB: The assumption that $T_v' \approx T_s'$ for a sonic anemometer is based on Kaimal (1990).

Output data: convective temperature scale from sonic anemometers at different heights, $\Theta_*(z)$. Data are not quality controlled.

7.5.14 Turbulent Kinetic Energy

Turbulence kinetic energy (TKE) is a measure of the energy in the turbulent velocity fluctuations that includes all three velocity components, rather than the turbulence intensity which only includes the stream-wise component. The instantaneous TKE is defined as:

$$\mathrm{TKE}(t) = \frac{1}{2}\left[u'u' + v'v' + w'w'\right] \tag{7.17}$$

and the mean over an interval is defined as:

$$\overline{\mathrm{TKE}} = \frac{1}{2}\left[\overline{u'u'} + \overline{v'v'} + \overline{w'w'}\right] \tag{7.18}$$

Output data: mean and peak TKE from sonic anemometers at different heights.

Source: Stull (1988), p. 46, eqn. 2.5c.

7.5.15 Coherent Turbulent Kinetic Energy

Coherent turbulent kinetic energy (CTKE) is a significant contributor to turbine loads. It is defined at an instant as

$$\mathrm{CTKE} = \frac{1}{2}\left([u'w']^2 + [u'v']^2 + [v'w']^2\right)^{1/2} \tag{7.19}$$

Output data: peak CTKE from sonic anemometers at different heights.

Source: Kelley (2011).

7.5.16 Turbulence time and length scales

The turbulence integral length scale (Λ) for a velocity component (u', v' or w') is calculated from the time series of the turbulent velocity component. It is measure of the eddy scales within the flow.

Three different methods are used to estimate the integral length scales, τ:

1. Integrating the autocorrelation function of u' over positive lags up to the first zero crossing
2. Calculating the peak in the 10-minute spectra, and dividing the period by 4

3. Fitting 10-minute spectral estimates to an equation for the Kaimal spectral shape

These are described in more detail in Pichugina et al. (2008).

The integral length scale is calculated as the product of the characteristic time derived by the different methods, and the mean wind speed. For the streamwise component, the integral length scale is:

$$\Lambda\left(u'\right) = U_{AD} \times \tau\left(u'\right) \tag{7.20}$$

NB: several studies have shown that the integral length scale is partly a function of the method used to derive it (e.g. Pichugina et al., 2008), while the integral length scale may be defined differently for different purposes. The reader is cautioned to use the appropriate length scale from the above methods.

Output data: integral length scales for the streamwise, lateral and vertical flow using different metrics from sonic anemometers at different heights.

Source: These values are calculated using the same code as was used in Pichugina et al. (2008).

7.5.17 Structure functions of velocity and temperature

The structure function describes the spatial correlation between a parameter and the convecting wind field. The structure functions of temperature and velocity have important implications for the performance of remote wind sensing (particularly SODAR, see Bradley, 2008) and can be used to estimate the dissipation rate.

The structure function for velocity (D_{VV}) for a time δt is the mean squared difference between u' at times t and δt:

$$D_{VV}\left(\delta t\right) = \overline{\left[u'\left(t+\delta t\right) - u'\left(t\right)\right]^2} \tag{7.21}$$

Similarly, a structure function can be calculated for temperature. This is denoted D_{TT}:

$$D_{TT}\left(\delta t\right) = \overline{\left[T'\left(t+\delta t\right) - T'\left(t\right)\right]^2} \tag{7.22}$$

A structure function parameter C_{AA} can be defined from the structure function. This is the ratio of the structure function to the cube root of the lag, and is a measure of the strength of turbulence, or magnitude of the temperature fluctuations:

$$C_{V^2}\left(\delta t\right) = \left[\frac{D_{VV}\left(\delta t\right)}{\left(U_{AD}\delta t\right)^{\frac{2}{3}}}\right] \tag{7.23}$$

$$C_{T^2}\left(\delta t\right) = \left[\frac{D_{TT}\left(\delta t\right)}{\left(U_{AD}\delta t\right)^{\frac{2}{3}}}\right] \tag{7.24}$$

where C_{V^2} is the structure function parameter for velocity, and C_{T^2} is the structure function parameter for temperature.

Output data: structure function of velocity and temperature from sonic anemometers at different heights, $C_{V^2}\left(z\right)$ and $C_{T^2}\left(z\right)$.

Source: Stull (1988), p. 300.

7.5.18 Dissipation rate

The dissipation rate ε is the rate at which turbulent kinetic energy is dissipated into heat at the smallest eddy scale in turbulent flow. Because this occurs at higher frequencies than can be resolved directly by the sonic anemometers, it has to be inferred from the turbulent power spectra.

In this case, we calculate ε from the sonic anemometer data using the structure function method described in Stull (1988). The dissipation rate ε is calculated from the structure function parameter for velocity:

$$\varepsilon = \left[\frac{\overline{C_{V^2}}}{2}\right]^{3/2}. \tag{7.25}$$

where the $\overline{C_{V^2}}$ is the median value of the velocity structure function parameter.

Figure 18 shows an example of the results. The dissipation rate is limited to the inertial subrange by using $0.05 \leq \delta t \leq 2$, corresponding to frequencies between 0.5 and 20 Hz. From power spectra of the turbulent velocity components (not shown), this is in the inertial subrange where energy cascades from the larger scales to smaller scales at a constant rate.

Output data: dissipation rate from sonic anemometers at different heights $\varepsilon(z)$.

Source: Stull (1988), p. 300.

7.6 Derived values

Derived values are values that require quality-controlled data from more than one instrument. The derived data inherit the quality codes of the data that are used in the calculation. For example, the wind speed and direction (see following section) requires quality-controlled data from co-located cups and vanes, and will inherit their quality codes.

7.6.1 Wind Direction (cups and vanes)

In order to calculate the mean wind speed and direction, the instantaneous measured wind speed u_c and direction WD are converted into orthogonal components. These orthogonal components are aligned south-north (v_m) and west-east (u_m), also known as meteorological zonal and meridional winds:

$$u_m = -u_c \sin\left(WD\tfrac{\pi}{180}\right) \tag{7.26}$$

$$v_m = -u_c \cos\left(WD\tfrac{\pi}{180}\right) \tag{7.27}$$

The mean wind direction is

$$\overline{WD} = \frac{180}{\pi} \times \arctan\left(\frac{\overline{-u_m}}{\overline{-v_m}}\right). \tag{7.28}$$

The standard deviation of the wind direction is:

$$\sigma(WD) = \arcsin(\varepsilon_{WD})\left[1 + \left(\frac{2}{\sqrt{3}} - 1\right)\varepsilon_{WD}^3\right] \tag{7.29}$$

where the expression $(2/\sqrt{3}) - 1 = 0.1547$, and

$$\varepsilon_{WD} = \left[1 - \left(\overline{\left(\frac{u_m}{u_{Cup}}\right)}^2 + \overline{\left(\frac{v_m}{u_{Cup}}\right)}^2\right)\right]^{1/2} \tag{7.30}$$

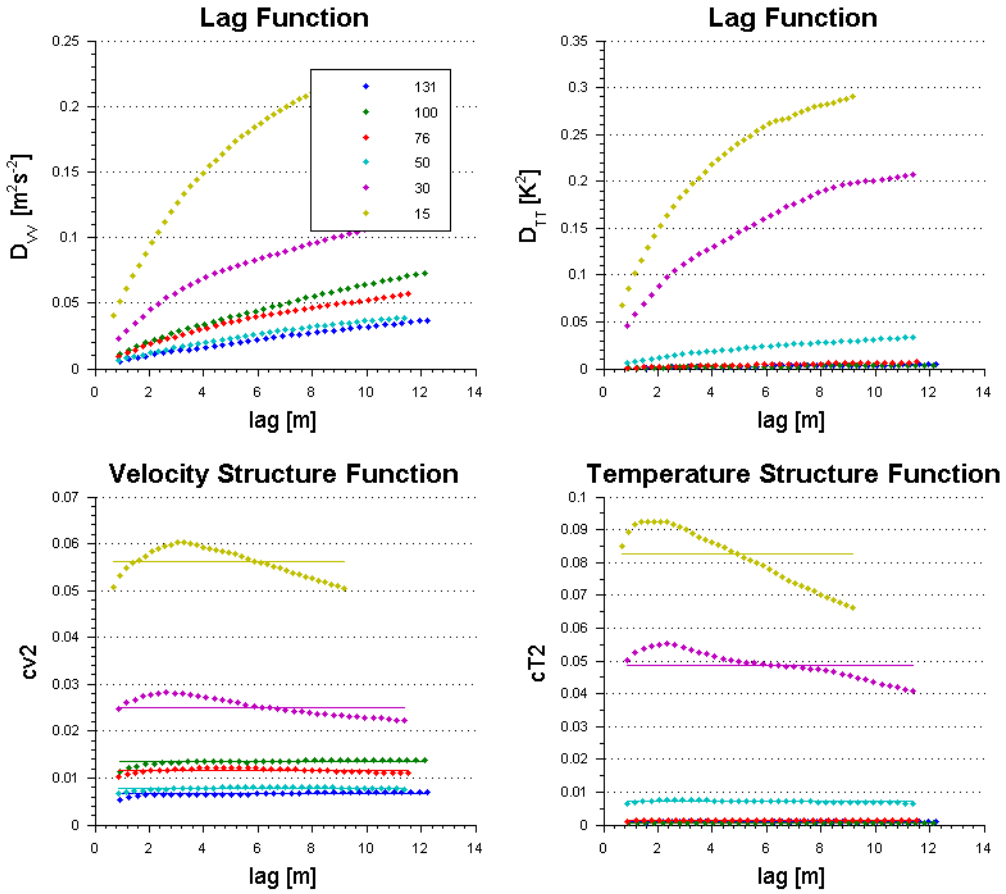

Figure 18. Example dissipation rate calculations. This figure was automatically generated during the processing of data from the 10-minute interval starting April 1, 2012, 03:30 UTC.

Output data: mean and standard deviation of wind speed and direction.

Source: Yamartino (1984).

7.6.2 Power-law velocity profile exponent (cups)

Wind shear α is a measure of the variation in wind speed as function of height. It is used in the power law to define the variation in mean cup wind speed with height, such that

$$U_{cup}(z) = \beta z^{\alpha} \tag{7.31}$$

This can be expressed as a linear function of two natural logarithms;

$$\ln\left[U_{cup}(z)\right] = \alpha \ln(z) + \ln(\beta) \tag{7.32}$$

The power law exponent α is therefore the gradient of a line fit by the least squares method to the log of the wind speed (y), and the log of the height (x). In this case, the fit is made using the MATLAB function `polyfit()` with a first-order polynomial.

The exponent is not constrained as a wide range of wind shear can occur under non-neutral conditions.

Output data: α for combinations of cup anemometers at different heights.

Source: Stull (1988).

7.6.3 Log-law friction velocity and roughness length (cups)

The log law defines the variation in time-averaged wind speed with height (in this case it is the mean cup wind speed, $U_{cup}(z)$) as a function of friction velocity u_* and roughness length z_0. The velocity profile is defined as

$$U_{cup}(z) = \frac{u_*}{\kappa} \ln\left(\frac{z}{z_0}\right). \tag{7.33}$$

As with the shear, Eq. 7.33 can be expressed as a linear function;

$$U_{cup}(z) = \frac{u_*}{\kappa} \ln z - \frac{u_*}{\kappa} \ln z_0. \tag{7.34}$$

The friction velocity and roughness length are found using a first-order polynomial fit to $y = \ln\left[U_{Cup}(z)\right]$, $x = z$ (i.e a linear least-squares fit), using the MATLAB function `polyfit()`. The gradient of the fit is $u_* \kappa$ and the intercept is $\frac{u_*}{\kappa} \ln z_0$.

NB: The roughness length and friction velocity are calculated only for mean wind speeds derived from cups and vanes.

If the fit does not converge or either value of u_* or z_0 is negative, both the friction velocity and roughness length are set to NaN.

Output data: u_* and z_0 for combinations of cup anemometers at different heights.

Source: Stull (1988).

7.6.4 Wind veer (vanes)

Wind veer is the variation in wind direction from one height to another, also known as wind direction shear. It is calculated as the mean rate of change of wind direction with height, between two heights.

Output data: wind veer calculated from all wind vanes between two heights.

7.6.5 Rain

The rain sensor quantifies rain as having intensity from 0 (heavy rain) to 3 (dry). A mean value of 2.7 or less implies either short duration, but heavy precipitation, or sustained light precipitation.

Some sonic anemometer data may be impacted by precipitation, in particular vertical velocity components. The user may wish to filter out sonic anemometer data where the mean rate during a 10-minute interval is less than 2.7. The precise threshold may vary depending on the reason for the filtering.

Output data: mean rain sensor reading in a 10-minute interval.

7.6.6 Air temperature profile

A high-accuracy air temperature profile is calculated as the sum of the mean temperature measured at the mast base, and the mean of the differential temperatures measured on the mast. For example, the mean temperature at 134 m is the sum of the mean temperature at 3 m, plus the mean temperature differential from 3 to 88 m, plus the mean temperature differential from 88 to 134 m.

Output data: mean air temperature at height z.

7.6.7 Saturation vapor pressure

The local saturation vapor pressure e_s is calculated at each height from the calculated air temperature $T(z)$ *in degrees Celsius*:

$$e_s(z) = 6.11 \times 10^{[(T(z)\cdot A)/(T(z)+B))} \tag{7.35}$$

where A =7.5 and B = 237.3 if $T(z) \geq 0°C$. Otherwise, A = 9.5 and B = 265.5.

Output data: The saturation vapor pressure is not output, but is used in subsequent calculations. The saturation vapor pressure inherits the quality codes of the calculated air temperature at each height.

7.6.8 Vapor pressure

The vapor pressure $e(z)$ is calculated from Eq. (7.35) by replacing $T(z)$ with the dew point temperature $T_d(z)$ in degrees celsius.

Output data: The vapor pressure is not output, but is used in subsequent calculations. The vapor pressure inherits the quality codes of the calculated air temperature at each height.

7.6.9 Relative humidity

The relative humidity ϕ is the relative vapor pressure, expressed as a percentage of the saturation vapor pressure:

$$\phi = 100 \times \frac{e(z)}{e_s(z)} \tag{7.36}$$

Output data: relative humidity at height z.

7.6.10 Specific humidity

The specific humidity q is the ratio of mass of water vapor to the total mass of the air (Garratt, 1994). It is calculated from the ratio of the local saturation vapor pressure, and actual local vapor pressures:

$$q = 0.622\frac{e}{P} \tag{7.37}$$

where 0.622 is the ratio of the gas constant for dry air (287 J Kg^{-1} K^{-1}) to the gas constant for water vapor (461.5 J Kg^{-1} K^{-1}).

Output data: The specific humidity is not recorded in the output data, but is used internally for other calculations. The specific humidity inherits the quality codes of the ground pressure and local vapor pressure.

7.6.11 Virtual temperature

The virtual temperature T_v is:

$$T_v = T\,(1+0.61q) \tag{7.38}$$

Output data: the virtual temperature is not recorded in the output data, but is used internally for other calculations. The virtual temperature inherits the quality codes of the air temperature and specific humidity.

Source: Garratt (1994).

7.6.12 Pressure gradient

The virtual temperature at the lowest height, T_{v0}, and barometric pressure are used to calculate the pressure gradient, dP/dz from the equation of state:

$$\frac{dP}{dz} = -\frac{gP_0}{RT_{v0}} \tag{7.39}$$

where g is the acceleration due to gravity (9.81 m s^{-2}) and R is the gas constant of dry air.

Output data: the pressure gradient is not recorded in the output data, but is used internally for other calculations. The pressure gradient inherits the quality codes of the ground pressure and virtual temperature at the lowest measurement point.

Source: Garratt (1994).

7.6.13 Pressure profile

The pressure profile $P(z)$ is a function of the mast-base pressure P_0, the height at which this is measured ($z(P_0)$) and the pressure gradient dP/dz:

$$P(z) = P_0 + (z - z(P_0))\frac{dP}{dz} \tag{7.40}$$

Output data: air pressure at different heights $P(z)$.

7.6.14 Potential temperature

The potential temperature Θ is the temperature that air at the ground would have if moved to a reference pressure level, $P_{ref} = 1000$ hPa. Calculating the potential temperature requires the pressure profile to be known:

$$\Theta(z) = T(z)\left[\frac{P_{ref}}{P(z)}\right]^{R/C_p} \tag{7.41}$$

where C_p is the specific heat capacity at constant pressure (1005 J Kg^{-1} K^{-1}). The ratio $R/C_p = 0.286$.

Output data: potential temperature at different heights $\Theta(z)$.

Source: Garratt (1994).

7.6.15 Virtual potential temperature

The virtual potential temperature Θ_v is the potential temperature that dry air air would require to have the same density as moist air. The virtual potential temperature is:

$$\Theta_v(z) = \Theta(z)(1 + 0.61q(z)) \tag{7.42}$$

where Θ is the 10-minute mean potential temperature at height z (Eq. 7.41), and q is the specific humidity at height z (Eq. 7.37).

Output data: virtual potential temperature at different heights $\Theta_v(z)$.

Source: Garratt (1994).

7.6.16 Gradient Richardson Number

The gradient Richardson number Ri is calculated from 10-minute average temperatures and gradients of wind components and virtual potential temperature between two heights (z_1 and z_2). The Richardson number can then be considered representative of the entire layer between z_1 and z_2. The gradient Richardson number is:

$$Ri = \frac{g}{\overline{\Theta_v}} \frac{d\overline{\Theta_v}/dz}{(d\overline{u_m}/dz)^2 + (d\overline{v_m}/dz)^2} \tag{7.43}$$

As was noted in the introduction, similar methods are used to analyze the data from the 135-m masts as are used on the 'M2' mast at the NWTC. Following the code documented in Johnson and Kelley (2000), the gradients of virtual potential temperature and speed between z_1 and z_2 are defined as the arithmetic mean of all measured gradients between z_1 and z_2. For example, consider the case where instruments measuring parameter y are uniformly separated by δz m in the interval z_1 to z_2. There will be n instruments, defining $n-1$ layers. The mean gradients will be

$$\overline{\frac{dy}{dz}} = \frac{1}{n-1}\sum_{i=1}^{n-1}\frac{y(i+1) - y(i)}{\delta z} \tag{7.44}$$

The Richardson number is calculated using wind speed and direction data from the cups and vanes.

Output data: Ri between different levels.

Source: Stull (1988).

7.6.17 Speed Richardson number

A simplified Richardson number has also been used in some applications. This definition considers just the gradient of the mean horizontal wind speed rather than including directional shear as in Eq. (7.43). To distinguish this Richardson number from the gradient Richardson number, this Richardson number is described as the 'Speed Richardson Number', and denoted Ri_S.

In this case, the relevant wind speed is the horizontal mean vector during the averaging period. Using data from the cups and vanes, the horizontal mean vector is calculated from the mean meridional and zonal wind components:

$$U_{c,vAD} = \left[\overline{u_m}^2 + \overline{v_m}^2\right]^{1/2} \tag{7.45}$$

The Speed Richardson number is then:

$$Ri_S = \frac{g}{\overline{\Theta_v}} \frac{d\overline{\Theta_v}/dz}{\left(dU_{c,vAD}/dz\right)^2} \tag{7.46}$$

As with the gradient Richardson number, the gradients of temperature ($d\overline{\Theta_v}/dz$) and speed (dU_{Cup}/dz) are the arithmetic mean of the gradients between heights z_1 and z_2.

NB: If $|Ri_S| > 10$, values are constrained to $10 \cdot Ri_S/|Ri_S|$. Data where $|Ri_S| > 10$ are flagged.

Output data: Ri_S between different levels.

Source: Businger et al. (1971); Grachev and Fairall (1997); Vickers and Mahrt (2004).

7.6.18 Brunt-Väisälä frequency

The Brunt-Väisälä frequency N is a measure of the oscillation frequency of turbulent eddies in the stable atmosphere. It is calculated from the potential temperature at two heights:

$$N^2 = \frac{g}{\frac{1}{2}\left(\Theta_v(z_1) + \Theta_v(z_2)\right)} \left[\frac{\Theta_v(z_2) - \Theta_v(z_1)}{z_2 - z_1}\right] \tag{7.47}$$

The Brunt-Väisälä frequency is calculated using wind speed and direction data from the cups and vanes.

NB: The Brunt-Väisälä frequency N^2 shares the sign of the Richardson number.

Output data: Brunt-Väisälä frequency (N) between heights $z1$ and $z2$.

7.6.19 Heat Flux

The local heat flux Q is defined from eddy covariance theory as:

$$Q = \rho C_p \overline{w' T_v'} \tag{7.48}$$

High-frequency measurements of the virtual temperature T_v are not available. Instead, noting that turbulent fluctuations of temperature measured by a sonic anemometer approximate the turbulent component of the virtual temperature; i.e. $T_s' \approx T_v'$, we use:

$$Q_s = \rho C_p \overline{w' T_s'} \tag{7.49}$$

where ρ is the air density at the height of the sonic anemometer. The air density is calculated by linearly interpolating the air density derived from temperature, pressure and humidity profiles to the sonic anemometer height.

NB: The assumption that $T_v' \approx T_s'$ for a sonic anemometer is based on Kaimal (1990).

7.6.20 Monin-Obukhov length

The Monin-Obukhov length, L is used to quantify stability. It is the height at which shear-driven turbulence is equal to buoyancy-generated turbulence:

$$L = -\frac{u_*^3}{\kappa g}\frac{T_v}{\overline{w'T_v'}} \tag{7.50}$$

where $\overline{w'T_v'}$ is the virtual temperature flux. However, T_v' is not available and instead the variation of the sonic temperature (T_s') is used:

$$L = -\frac{u_*^3}{\kappa g}\frac{T_v}{\overline{w'T_s'}} \tag{7.51}$$

where $\overline{w'T_s'}$ is measured by the sonic anemometer nearest the ground.

The potential temperature in Eq. (7.51), T_v, is calculated by linearly interpolating the derived potential temperature profiles to the height of the sonic anemometer. Note that the virtual potential temperature is *not* used because the Monin-obukhov length is related to local heat transfer and has no relation to the altitude at which the measurements are made.

The Monin-Obukhov length is frequently normalized by the measurement height z to give the ratio $\zeta = z/L$ (see e.g. Oncley et al., 1996). Locally convective conditions are characterized by $\zeta < 0$, and stable conditions by $\zeta > 0$, while in neutral conditions, $L \to \infty$ and thus $\zeta \to 0$. However, the actual boundaries between different atmospheric stratification states are usually defined by the author depending on their requirements, and so ζ is not mapped to a specific state (i.e. there is no output data that encodes $\zeta > 0$ as 'stable').

NB: The assumption that $T_v' \approx T_s'$ for a sonic anemometer is based on Kaimal (1990).

Output data: Monin-Obukhov length L and normalised Monin-Obukhov length, ζ.

Source: Foken (2006); Oncley et al. (1996).

8 Tower Performance Tests

The tower operation has been confirmed by a series of tests that checked the ability of the tower to correctly acquire data and process it such that the data correspond to available independent measures of the same variables.

8.1 Data storage and archiving

Tests have been made to check the ability to accurately store and retrieve data. These checks include:

- Unpacking binary data files from the met tower and comparing them to text files written by the data acquisition system in the same period. This confirms the ability to compress and unpack tower data files.
- Comparing MATLAB raw data files to tower text files. This confirms the ability to correctly unpack and store tower data in a new format, and that channels are correctly identified (i.e. no mix-up between barometric pressure and wind direction).
- Retrieve data and deliver to users. Data files for several months have been concatenated and delivered to selected external partners, where data have been used for various purposes. This confirms that the data files are transportable.

8.2 Data comparisons

Several comparisons have been made between data measured on the towers and other data sources at the NWTC (Figure 2). The following section is a qualitative comparison of the 135-m tower data with these alternative data sources. A quantitative comparison is planned but is outside the scope of this document.

8.2.1 M4 - M2 comparisons

The M2 tower is approximately 1500 m WSW of the M4 tower (Figure 2). Because of the separation, data at the M2 and M4 towers should not be expected to be identical, but the following trends should be apparent if the instrumentation, data acquisition systems and data processing are working well:

- Comparable wind speed and temperature
- Similar ramps of wind speed and temperature
- Similar diurnal cycles of wind speed, temperature, relative humidity and stability

Data are also not strictly comparable as the M2 data are calculated over 1-minute intervals, while the M4 data are for 10-minute intervals. Because of the different averaging periods, trends are compared qualitatively rather than quantitatively.

8.2.1.1 Wind speed and direction

The wind speed and direction at 80 m on the M2 tower with the M4 tower are very similar for the period chosen. Wind speeds are typically within 0.5 m s^{-1} of each other, and wind directions are within 10° (Figure 19). Ramp events (large changes in wind speed over short periods of time) are seen at both towers, while changes in wind direction also occur within a short time at each tower. Occasional differences in wind speed are observed (e.g. midday, 4/13) when the wind direction is not aligned with the towers.

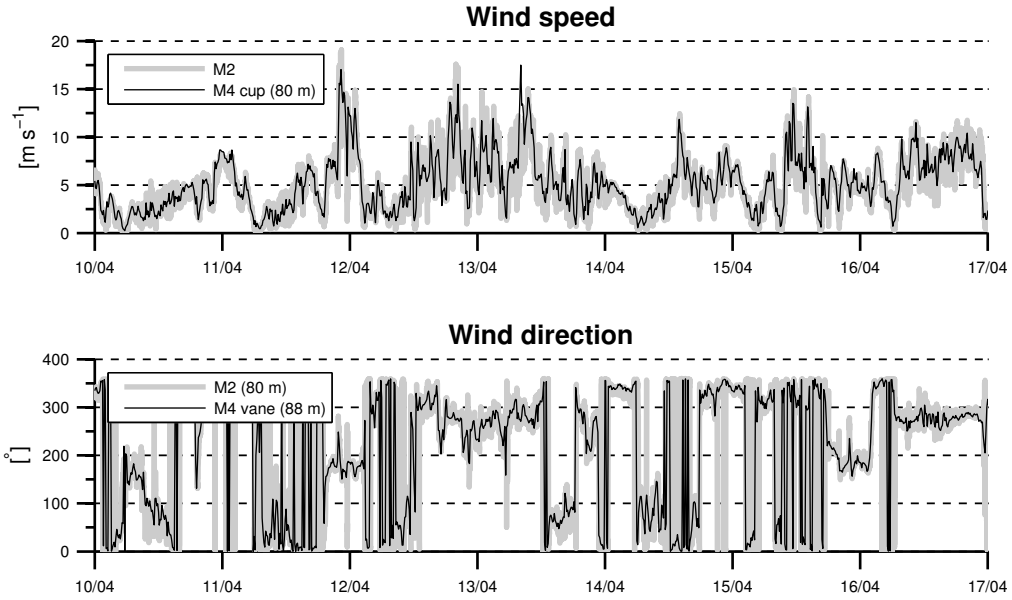

Figure 19. Wind speed and direction at the M2 and M4 towers. Data are taken for an arbitrary 1-week period in Spring 2012, when there is considerable variation in wind speed and direction.

8.2.1.2 Air temperature and humidity

A similar comparison was made between the air temperature and humidity on the M2 and M4 towers (Figure 20). As with the wind direction and wind speed (Figure 19), very close agreement is seen between the M2 and M4 towers.

8.2.1.3 Stability

The atmospheric stability at the M2 tower is quantified using a wind speed-gradient Richardson number Ri_S, as described in Section 7.6.17. The diurnal cycle of stability is clearly visible at both the M2 and M4 towers (Figure 21). Some difference is seen in the magnitude of stability at the M2 and M4 locations, but not the sign (positive or negative). The difference is not surprising, as the two towers are approximately 1 km apart (Figure 2), the M2 stability is calculated every minute rather than every 10 minutes as on the M4 tower, and sensors are at different heights and so the gradients at each location may be different.

8.2.2 M4 - SODAR Wind speed and direction comparison

A Second Wind 'Triton' SODAR system was also deployed at the NWTC during the same period as the data shown in Figure 19 was collected. The Triton is a monostatic SODAR system that uses acoustic pulses to probe the atmosphere and return wind speed and direction at different heights (Figure 22). An in-depth overview of SODAR technology is given in Bradley (2008).

The SODAR was deployed approximately 400 m upwind of the M4 tower on a bearing of 270°. The Triton is a commercially-available system that is completely independent of the systems at the NWTC. Data is managed separately and is downloaded from an online database. Because of the relative proximity of the tower and SODAR but different data processing methods, fundamental errors with the M4 data processing systems should be apparent if

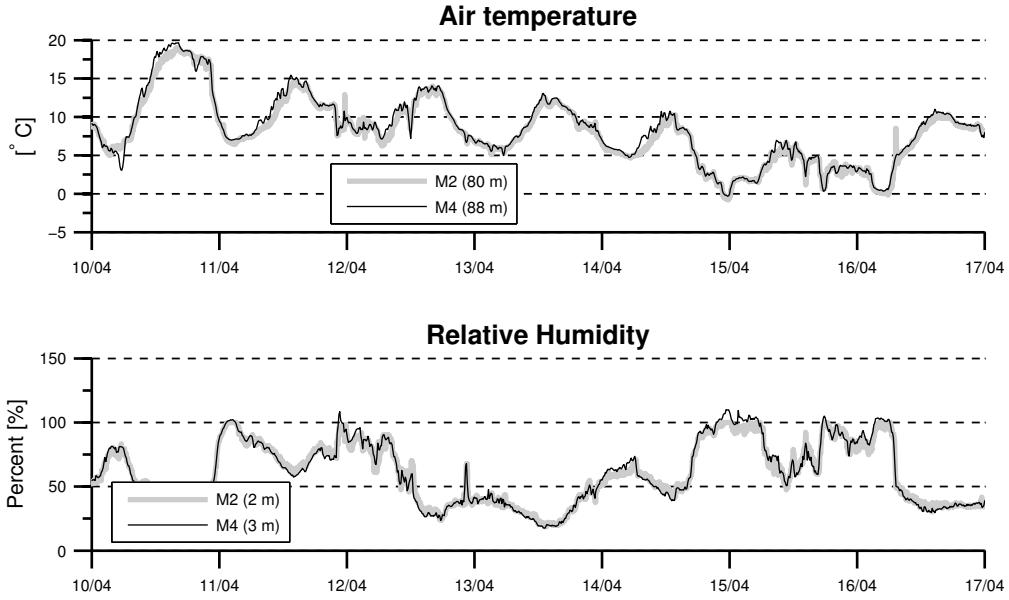

Figure 20. Air temperature and relative humidity at the M2 and M4 towers. Data are taken for the same 1-week period in Spring 2012 as Figure 19.

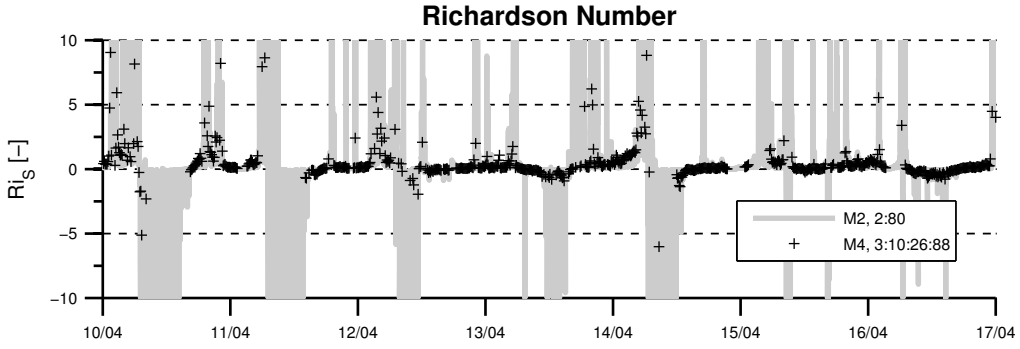

Figure 21. Speed-gradient Richardson number at the M2 and M4 towers. Data are taken for the same period as Figure 19.

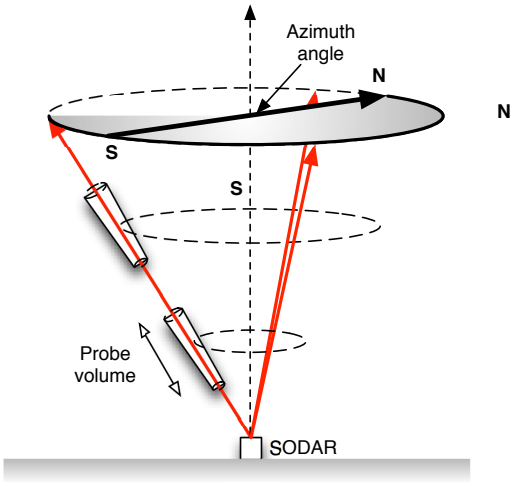

Figure 22. Vertically-profiling SODAR.

the SODAR and M4 data are compared. As figure 23 shows, the M4 and SODAR agree well, with both systems detecting similar wind speeds and wind direction, as well as similar transients.

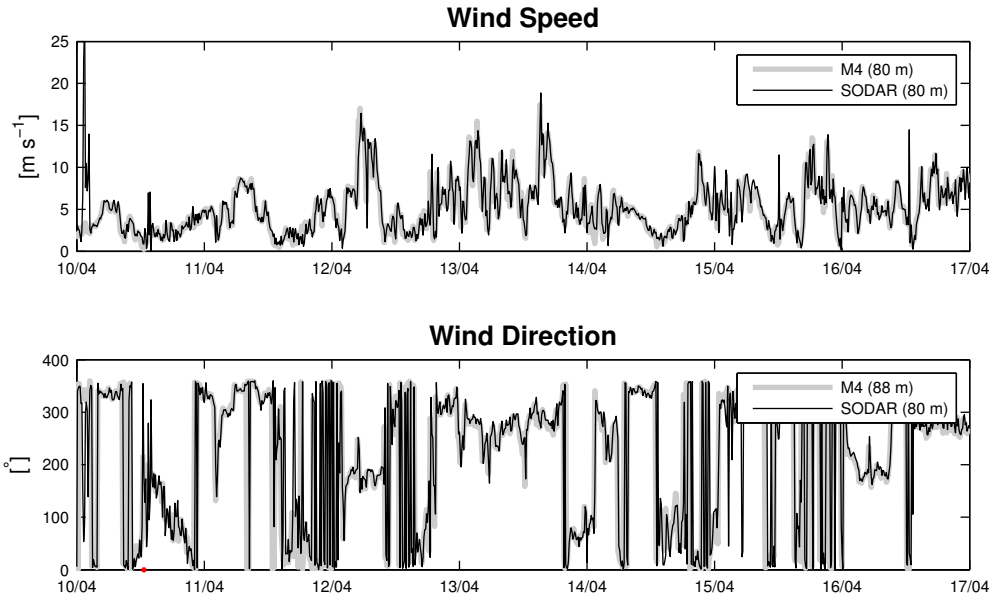

Figure 23. Wind speed and direction from a SODAR and the M4 tower. Data are taken for the same period as Figure 19.

9 Outlook and Future Work

Two new, 135-m meteorological masts have been installed and are being commissioned at the National Wind Technology Center near Denver, Colorado. These masts are heavily instrumented to measure the bulk and local properties of the atmosphere, including winds, turbulence and thermodynamics.

The masts will be used for a variety of purposes. These include:

- Inflow characterization
- Remote sensing characterization and verification
- Supporting other observations

Continued operation will benefit the United States' wind industry through better understanding of the effects of turbulent inflow on wind turbine performance; through better use of remote sensing devices and data; and through more observations of a wider range of atmospheric conditions and the effect of those conditions on turbine performance.

9.1 Inflow Characterization

The masts were designed primarily to measure the winds flowing into the utility-scale wind turbines directly downwind. This work has already started and includes studies of the relationship between atmospheric stability and turbulence in the turbine layer (Clifton et al., 2012a, 2013b, 2012b), noise propagation (Medina et al., 2011), and turbine wake formation and propagation (Aitken et al., 2012; Lundquist et al., 2012).

The masts will be used to investigate the relationship between inflow conditions and turbine response. This will require synchronized measurements of inflow and turbine response at several different time scales. One area of investigation is the effect of changing turbulence on the turbines, for example the coherent turbulence that Kelley (2011) observed to be important in raising the loads on wind turbines. Another area of research will the effect of changes in the bulk flow field, such as shear, veer and wind speed on turbine performance. The response of a turbine to all of these effects (shear, veer, and turbulence) is essential information for wind turbine siting and operation.

The Center for Research and Education in Wind[1] awarded a grant in 2012 to use the masts to develop nacelle transfer functions. These transfer functions are methods by which measurements made on the turbine nacelle by the turbine's own instrumentation can be related to the upwind conditions. If a better estimate of the inflow can be made from those measurements resulting in improved performance or reduced loading, it may be possible to apply this to the entire wind turbine fleet.

9.2 Remote Sensing

The 135-m masts have been used to provide data for the verification and characterization of remote sensing devices. The masts have been used to measure wind speeds, direction and turbulence properties for comparison to the data from remote sensing devices (see e.g. Clifton et al., 2013a). Data from the masts have also been used to show changes in atmospheric conditions impact the performance of remote sensing devices in other ways, such as the ability of a device to get data at high-altitude, low-humidity sites.

Work is ongoing to compare data from remote sensors of thermodynamic properties with the data from the masts. An example of this is a comparison of data from a microwave radiometer with the thermodynamic profiles from the masts, which continues work described in Friedrich et al. (2012).

[1] CREW, see `http://crew.colorado.edu/`

9.3 Observation Support

Data from the 135-m masts are regularly used for other projects at the NWTC, while data are also shared with other researchers worldwide through the internet. Following the announcement in 2012 of the Department of Energy's plans to develop a reference facility for offshore renewable energy (RFORE, Cline et al., 2013), the masts are being used to test concepts for instrumentation on this offshore facility.

Bibliography

Aitken, M.L.; Lundquist, J.K.; Pollak, D.A.; Mirocha, J.D.; Banta, R.M.; Pichugina, Y.L.; Brewer, W.A.; Alvarez, R.J.; Sandberg, S.P.; Brown, J.M.; Kelley, N.D.; Clifton, A. (January 2012). "Characterization of Inflow Conditions and Wake Structures for a Wind Turbine in Complex Terrain Using Long-Range Doppler Lidar." *Third Conference on Weather, Climate, and the New Energy Economy*. American Meteorological Society.

Banta, R.; Olivier, L.; Gudiksen, P. (1993). "Sampling requirements for drainage flows that transport atmospheric contaminants in complex terrain." *Radiation Protection Dosimetry* 50(2-4); pp. 243–248.

Bradley, S. (2008). *Atmospheric acoustic remote sensing*. CRC Press.

Businger, J.A.; Wyngaard, J.C.; Izumi, Y.; Bradley, E.F. (2011/10/27 1971). "Flux-Profile Relationships in the Atmospheric Surface Layer." *Journal of the Atmospheric Sciences* 28(2); pp. 181–189.
URL `http://dx.doi.org/10.1175/1520-0469(1971)028<0181:FPRITA>2.0.CO;2`

Clifton, A.; Elliott, D.; Courtney, M., eds. (October 2013a). *Ground-based vertically-profiling remote sensing for wind resource assessment*. 1st ed. No. 15 in Expert Group Study on Recommended Practices, International Energy Agency.

Clifton, A.; Lundquist, J.K.; Kelley, N.D.; Scott, G.; Schreck, S.; Pollak, D.A.; Aitken, M.L.; Jager, D. (January 2012a). "Characterizing Inflow Conditions Across the Rotor Disk of A Utility Scale Wind Turbine." *Third Conference on Weather, Climate, and the New Energy Economy*. American Meteorological Society.

Clifton, A.; Schreck, S.; Scott, G.; Kelley, N.D.; Lundquist, J. (2013b). "Turbine Inflow Characterization at the National Wind Technology Center." *Journal of Solar Energy Engineering* 135(3).

Clifton, A.; Lundquist, J.K. (2012). "Data clustering reveals climate impacts on local wind phenomena." *Journal of Applied Meteorology and Climatology* 51; pp. 1547–1557.

Clifton, A.; Schreck, S.; Scott, G.; Kelley, N.; Lundquist, J.K. (2012b). "Turbine Inflow Characterization at the National Wind Technology Center." *Proceedings of the ASME 30th Wind Energy Symposium*. AIAA-2012-0658, AIAA.

Cline, J.; Shaw, W.J.; Clifton, A. (January 2013). The Chesapeake Light Tower: A New Reference Facility for Offshore Renewable Energy. Presentation.

Foken, T. (2006). "50 years of the Monin-Obukhov similarity theory." *Boundary-Layer Meteorology* .

Friedrich, K.; Lundquist, J.K.; Aitken, M.; Kalina, E.; Marshall, R.F. (02 2012). "Stability and turbulence in the atmospheric boundary layer: A comparison of remote sensing and tower observations." *Geophysical Research Letters* 39(3); p. L03,801.
URL `http://dx.doi.org/10.1029/2011GL050413`

Garratt, J. (1994). *The Atmospheric Boundary Layer*. 1st ed. Cambridge Atmospheric and Space Science Series, Cambridge University Press.

Grachev, A.A.; Fairall, C.W. (2011/10/01 1997). "Dependence of the Monin–Obukhov Stability Parameter on the Bulk Richardson Number over the Ocean." *Journal of Applied Meteorology* 36(4); pp. 406–414.
URL `http://dx.doi.org/10.1175/1520-0450(1997)036<0406:DOTMOS>2.0.CO;2`

IEC (2005). *IEC 61400-12-1: Wind turbines - Part 12-1: Power performance measurements of electricity producing wind turbines*. 1st ed. Geneva, Switzerland: International Electrotechnical Commission.

Johnson, W.; Kelley, N. (2000). *Design Specifications for the Development of the Initial Validation Software (Version 3.0) for Processing of NWTC 80-Meter Meteorological Tower Data*. NREL/TP-500-27104, National Renewable Energy Laboratory.

Kaimal, J. (1990). *Sonic Temperature – significance and limitations*. WPL Application Note No.4.

Kelley, N.D. (2011). *Turbulence-Turbine Interaction: The Basis for the Development of the TurbSim Stochastic Simulator.* TP-5000-52353, National Renewable Energy Laboratory.

Lundquist, J.K.; Pichugina, Y.; Banta, R.M.; Kelley, N.D.; Aitken, M.; Alvarez, R.J.; Brewer, W.A.; Brown, J.M.; Clifton, A.; Mirocha, J.D.; Sandberg, S.P. (January 2012). "Four-Dimensional Characterization of Inflow to and Wakes From a Multi-MW Turbine: The Turbine Wake and Inflow Characterization Study." *Third Conference on Weather, Climate, and the New Energy Economy*. American Meteorological Society.

Medina, P.; Singh, M.; Johansen, J.; Jove, A.; Machefaux, E.; Fingersh, L.; S.Schreck (2011). *Aerodynamic and Performance Measurements on a SWT-2.3-101 Wind Turbine.* Conference Paper CP-5000-51649, National Renewable Energy Laboratory.

Oncley, S.P.; Friehe, C.A.; Larue, J.C.; Businger, J.A.; Itsweire, E.C.; Chang, S.S. (1996). "Surface-layer Fluxes, Profiles and Turbulence Measurements over Uniform Terrain under Near-Neutral Conditions." *Journal of the atmospheric Sciences* 53(7); pp. 1029–1044.

Pichugina, Y.L.; Tucker, S.C.; Banta, R.M.; Brewer, W.A.; Kelley, N.D.; Jonkman, B.J.; Newsom, R.K. (2012/10/26 2008). "Horizontal-Velocity and Variance Measurements in the Stable Boundary Layer Using Doppler Lidar: Sensitivity to Averaging Procedures." *Journal of Atmospheric and Oceanic Technology* 25(8); pp. 1307–1327.
URL http://dx.doi.org/10.1175/2008JTECHA988.1

Sadoud, M. (2012). *Lattice Tower Shadow Effect Investigation*. GL-GH 800113-CAMO-T-01, GL Garrad Hassan.

Stull, R. (1988). *An Introduction to Boundary Layer Meteorology*. 2nd ed. Kluwer Academic Publishers.

Tusch, M.; Masson, C.; Heraud, P. (2011). "Modeling of Turbulent Atmospheric Flow Around Tubular and Lattice Meteorological Masts." *Journal of Solar Energy Engineering* 133(1); p. 011,011.

Vickers, D.; Mahrt, L. (2011/10/01 2004). "Evaluating Formulations of Stable Boundary Layer Height." *Journal of Applied Meteorology* 43(11); pp. 1736–1749.
URL http://dx.doi.org/10.1175/JAM2160.1

Weber, R.O. (1999). "Remarks on the definition and estimation of Friction velocity." *Boundary Layer Meteorology* 93; pp. 197–209.

Wilczak, J.; Oncley, S.; Stage, S. (2001). "Sonic Anemometer Tilt Correction Algorithms." *Boundary-Layer Meteorology* 99; pp. 127–150.
URL http://dx.doi.org/10.1023/A:1018966204465

Wyngaard, J.C. (1981). "Cup, Propellor, Vane and Sonic Anemometers in Turbulence Research." *Annual Review of Fluid Mechanics* 13; pp. 399–423.

Yamartino, R.J. (2012/02/17 1984). "A Comparison of Several "Single-Pass" Estimators of the Standard Deviation of Wind Direction." *Journal of Climate and Applied Meteorology* 23(9); pp. 1362–1366.
URL http://dx.doi.org/10.1175/1520-0450(1984)023<1362:ACOSPE>2.0.CO;2

Index